THE EFFECT OF CRYSTALLOGRAPHIC ORIENTATION AND THERMO-MECHANICAL LOADING CONDITIONS ON THE PHASE TRANSFORMATION CHARACTERISTICS OF FERROMAGNETIC SHAPE MEMORY ALLOYS

A Thesis

by

RUIXIAN ZHU

Submitted to the Office of Graduate Studies of
Texas A&M University
in partial fulfillment of the requirements for the degree of

MASTER OF SCIENCE

December 2009

Major Subject: Mechanical Engineering

THE EFFECT OF CRYSTALLOGRAPHIC ORIENTATION AND THERMO-MECHANICAL LOADING CONDITIONS ON THE PHASE TRANSFORMATION CHARACTERISTICS OF FERROMAGNETIC SHAPE MEMORY ALLOYS

A Thesis

by

RUIXIAN ZHU

Submitted to the Office of Graduate Studies of
Texas A&M University
in partial fulfillment of the requirements for the degree of

MASTER OF SCIENCE

Approved by:

Chair of Committee,	Ibrahim Karaman
Committee Members,	Dimitris C. Lagoudas
	Richard Griffin
Head of Department,	Dennis O'Neal

December 2009

Major Subject: Mechanical Engineering

ABSTRACT

The Effect of Crystallographic Orientation and Thermo-Mechanical Loading Conditions on the Phase Transformation Characteristics of Ferromagnetic Shape Memory Alloys.

(December 2009)

Ruixian Zhu, B.A., Shanghai Jiao Tong University, China

Chair of Advisory Committee: Dr. Ibrahim Karaman

The effects of crystallographic orientation, temperature and heat treatment on superelastic response of $Ni_{45}Mn_{36.5}Co_5In_{13.5}$ single crystals were investigated. Superelastic experiments with and without various magnetic field were conducted under compression on a custom built magneto-thermo-mechanical test setup. Magnetostress, which is the difference in critical stress levels for the martensitic transformation with and without magnetic field, was determined as a function of crystallographic orientation, heat treatment and temperature parameters. Magnetostress of [111] crystals was observed to be much higher than that of [001] crystals with same heat treatment. Water quenched samples have the highest magnetostress among other samples with the same orientation that were oil quenched and furnace cooled. Crystal structure and atomic ordering of the samples were examined using Synchrotron High-Energy X-Ray Diffraction to rationalize observed differences. Magnetostress levels were also traced at various temperatures. A Quantum Design superconducting quantum interference device (SQUID) was utilized to examine the magnetic properties of the material. The difference in saturation magnetization at various temperatures was analyzed to explain the temperature effect on magnetostress. Calculations based on the energy conversion from available magnetic energy to mechanical work output were used to predict the magnetic field dependence of magnetostress, which provides a guideline in material selection for the reversible magnetic field induced martensitic phase transformation.

Isothermal superelastic response and load-biased shape memory response of $Co_{48}Ni_{33}Al_{29}$ single crystals were determined as a function of temperature and stress, respectively. The aim of the work is to provide a new direction to understand the anomaly of transformation strain and hysteresis for ferromagnetic shape memory alloys. Thermo-mechanical behavior of $Co_{48}Ni_{33}Al_{29}$ single crystal was determined by a custom built thermo-mechanical compression setup based on an electromechanical test frame made by MTS. Transformation strain was observed to decrease with increasing applied stress in isothermal tests or increasing temperature in superelastic experiments. The variation in the lattice constant in martensite and austenite was verified to account for such a trend. It was also discovered that both thermal and stress hysteresis decreased with increasing applied stress and temperature, respectively. Multiple factors may be responsible for the phenomenon, including the increase of dislocation, the compatibility between martensite and austenite phase.

To My Parents

ACKNOWLEDGEMENTS

First of all, I would like to thank my advisor, Prof. Ibrahim Karaman, who helped me in all aspects of the project. Without his patience and support, this project would have not been completed. Some of the suggestions were very helpful not only for the project, but also for any other research I may conduct in the future.

I would also like to thank my committee members, Prof. Richard Griffin and Prof. Dimitris Lagoudas, for their suggestions on my research.

I am grateful to Prof. Yuriy Chumlyakov for sharing knowledge about fundamental material science with me. I also want to thank Dr. Ren Yang for his help on XRD experiments.

Special thanks should be given to Dr. W. Ito, Dr. Umetsu and Prof. Kainuma for their help with SQUID experiments.

Finally, I would like to thank my labmates, Dr. Majld Al-Maharb, Micheal Murphy, Dr. Burak Basaran, Ji Ma, Kadri C. Atli, Nevin Ozdemir, Ebubekir Dogan, Erhan Akin, Fatmata Barrie and Cengiz Yegin. You made life so interesting in the lab.

TABLE OF CONTENTS

CHAPTER Page

LIST OF FIGURES

FIGURE Page

FIGURE Page

FIGURE Page

LIST OF TABLES

CHAPTER I
INTRODUCTION

Background and Outlines

Smart materials, often called multifunctional materials, have attracted much attention in the past decade. These materials, e.g. piezoelectrics, magnetostrictives, and shape memory alloys, usually have the ability to transform one kind of energy to another. For example, piezoelectric ceramics can convert mechanical energy into electric energy or vice versa [1]. Magnetostrictive materials can utilize magnetic field as a source to gain strain and realize the energy exchange [2, 3]. Some popular smart materials are shown in Figure 1-1. In figure 1-1, different groups of smart materials are classified by actuation stress and actuation strain. In general, electrostrictive ceramics and shape memory alloys can have the maximum actuation stress (or blocking stress) with about 1000 MPa [1, 4] while electroactive polymers [5] are able to reach a maximum about 50% strain upon the application of the stimulus, i.e. electric field, temperature or magnetic field. The lines in the figure indicate different level of output energy, which is simply the product of actuation stress and strain. Shape memory alloys can have an actuation work output of as much as 50MJ/m3[6], which is probably the largest output energy among other smart materials.

Actuation frequency is another critical parameter for smart materials. Figure 1-2 shows the specific actuation energy density as a function of actuation frequency for different class of smart materials. Here the specific actuation energy density means the output energy per unit mass of material. From figure 1-1, it is clear that shape memory alloys could achieve the largest output energy among other smart materials. In this figure, unfortunately, it can be found that the actuation frequency of shape memory alloys is fairly low (in the order of 10Hz). On the other hand, magnetostrictive materials have an extremely high actuation frequency (in the order of 10^4Hz) but a very low actuation strain (0.1%).

This thesis follows the style of Acta Materialia.

Magnetic shape memory alloys take the advantage of shape memory alloys and Magnetostrictive materials. Although they don't have an extremely high output energy or highest actuation frequency, they do have a fairly good performance in terms of both output energy and actuation strain, thus attracting much attention in the recent ten years. Also, the current study will be focused on this class of material.

The material in this thesis is arranged as follows. In Chapter I, a very brief introduction is first given on conventional shape memory alloys to show some basic and common properties of this class of materials, including magnetic shape memory alloys. Then some unique properties and deformation mechanisms are introduced for magnetic shape memory alloys followed by the specific objective and purpose of the current study. In Chapter II, experimental techniques are going to be briefly introduced, including the kinds of experiments that were conducted during the study. Chapter III will include the results and discussion on studying the orientation, heat treatment and temperature effect on the magnetostress of NiMnCoIn metamagnetic shape memory alloys. Chapter IV will show the results and discuss the effect of thermo-mechanical loading conditions on the transformation strain and hysteresis of CoNiAl bulk material. Finally, Chapter V is a conclusion of all the current work.

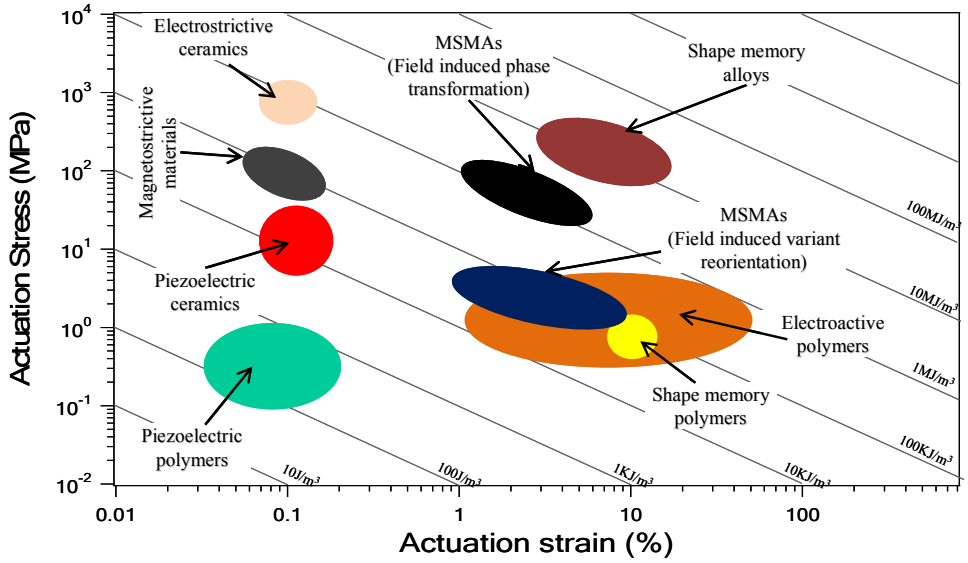

Figure 1-1 Actuation stress versus actuation strain for most popular smart materials

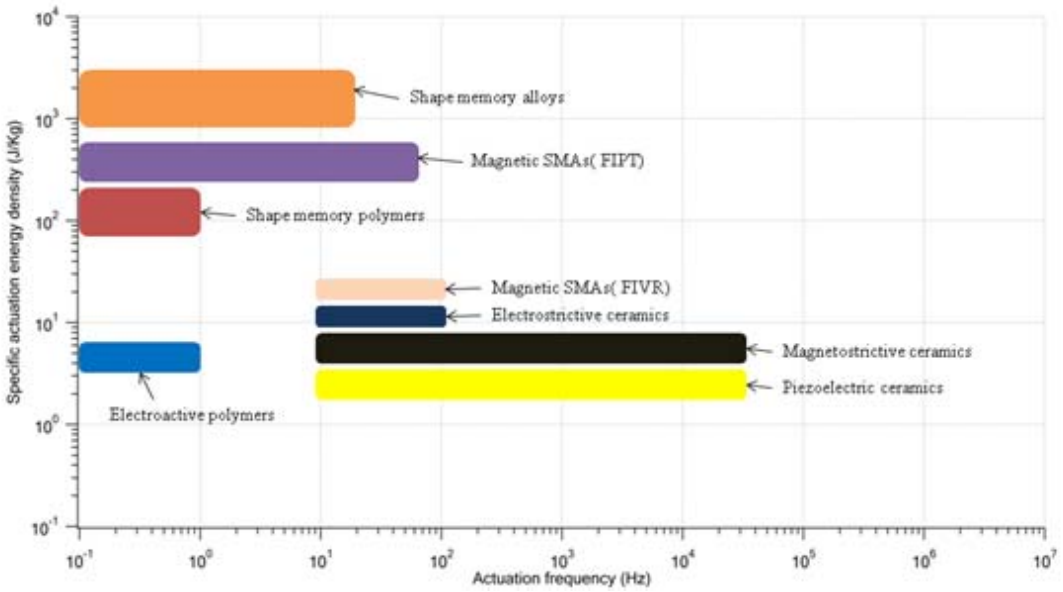

Figure 1-2 Actuation energy density of popular smart materials

Shape Memory Alloys

As mentioned above, here a very brief introduction of shape memory alloys will be present. First discovered in gold-cadminum alloy in 1932, shape memory alloys (SMAs) have received scientists' great attention for more than half a century [4]. Briefly speaking, SMA shows a thermal-mechanical coupling, which means they can convert thermal energy into mechanical work or vice versa. The actuation strain of SMAs is achieved by so called shape memory effect. Briefly speaking, the strain of SMAs can be collected by detwining martensite variants during martensite transformation and recovered upon heating procedure through reverse transformation. Here, martensite transformation plays a critical role in the shape memory effect. A more detailed description will be provided on the martensite transformation in the next section. A lot of alloy systems have been developed in the past years, such as CuZn [5], CuAl [6], AuCd [7], NiTi [8] and so on. Two main advantages are considered over other smart materials, high output stress (up to 10^3MPa for precipitate NiTi [9]) and large recoverable strain

due to the martensite transformation. Also, since SMA can reach relative high output stress and strain at the same time, high output energy can be collected (in the order of MJ/m^3) and thus making SMA a good material for energy harvesting and actuation applications.

Martensitic Transformation

Martensite is named after a German scientist Martens. It was first used to describe the microconstituent phase in quenched steels. After that, many other materials have been discovered to exhibit martensitic transformation, including SMAs. In fact, martensitic transformation and its reversal is the reason for the recoverable shape change.

Figure 1-3 shows the experimental observation of martensite morphology using optical microscopy by C.M.Wayman [10]. The sample is Fe-24.5Pt at.% alloy and is transformed into martensite by cooling. The specimen was polished flat prior to transformation. The alternating light and dark regions within the grains are all martensites. The reason for the contrast is the distortion of martensites in different directions with respect to the surface.

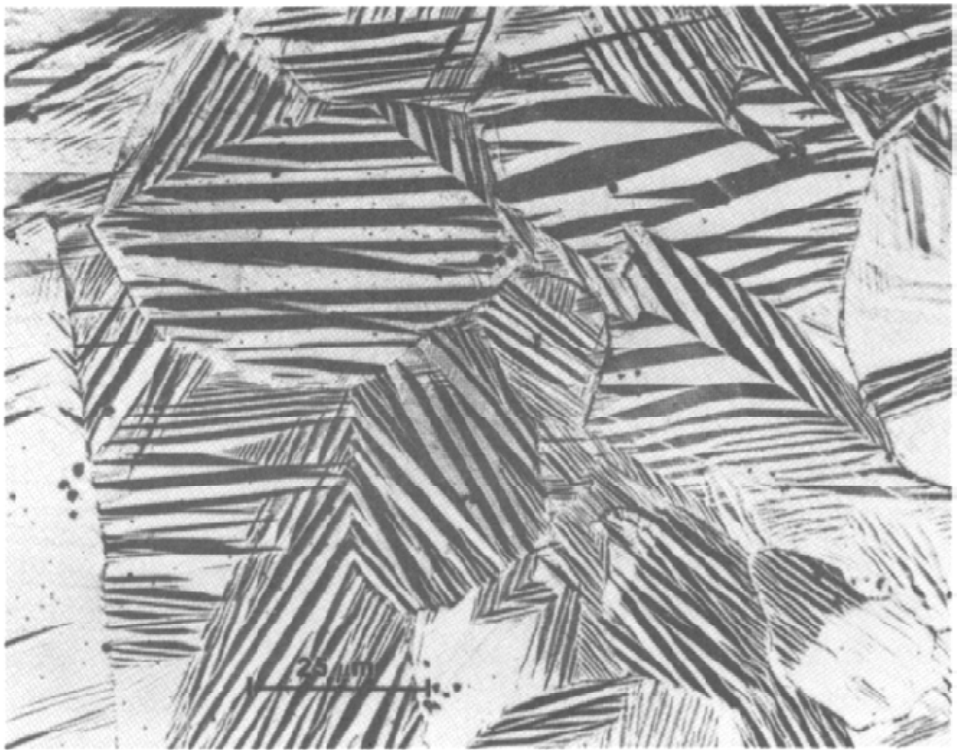

Figure 1-3 Optical microscopy picture of martensite plates in Fe-24.5Pt at wt% alloy[10]

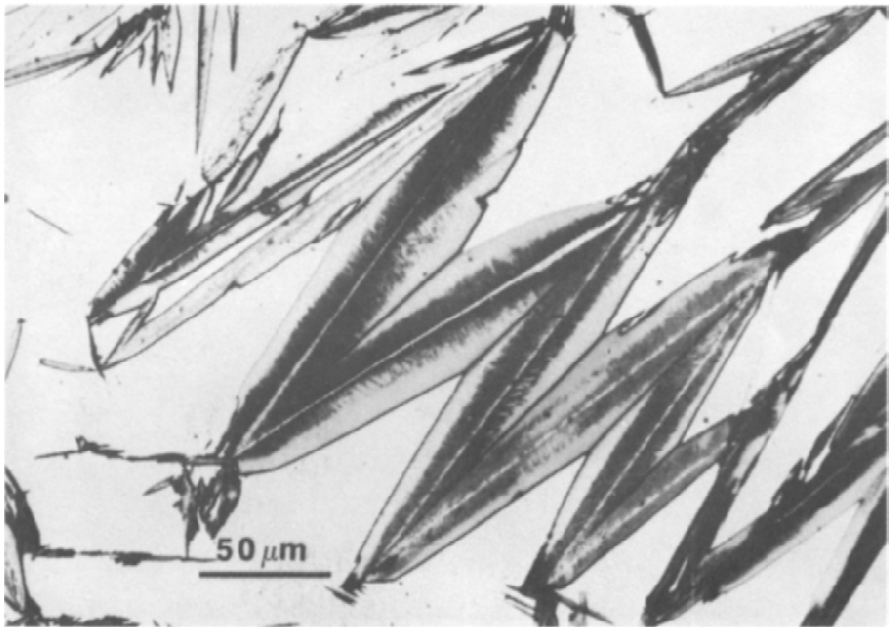

Figure 1-4 Martensites with lenticular plates morphology under optical microscorpy[10]

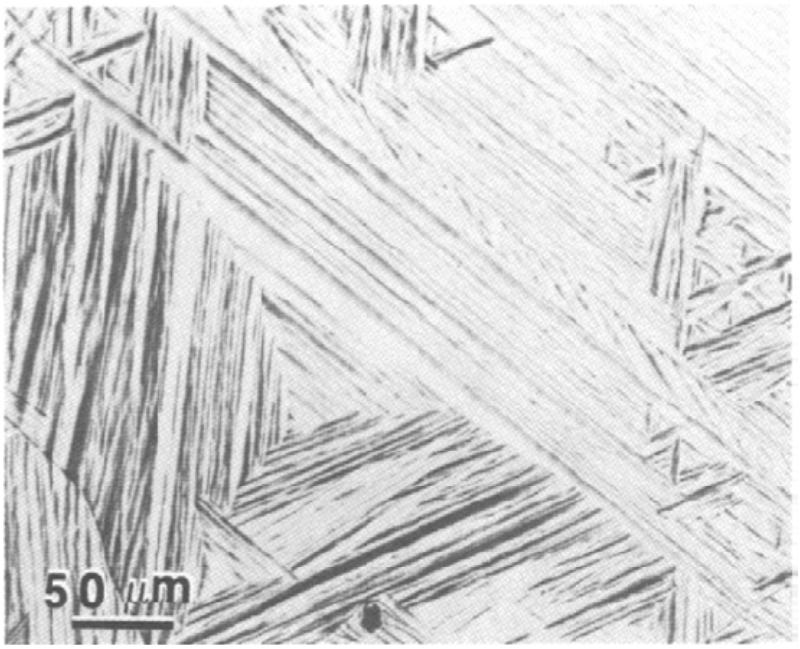

Figure 1-5 Martensites with lath morphology under optical microscopy[10]

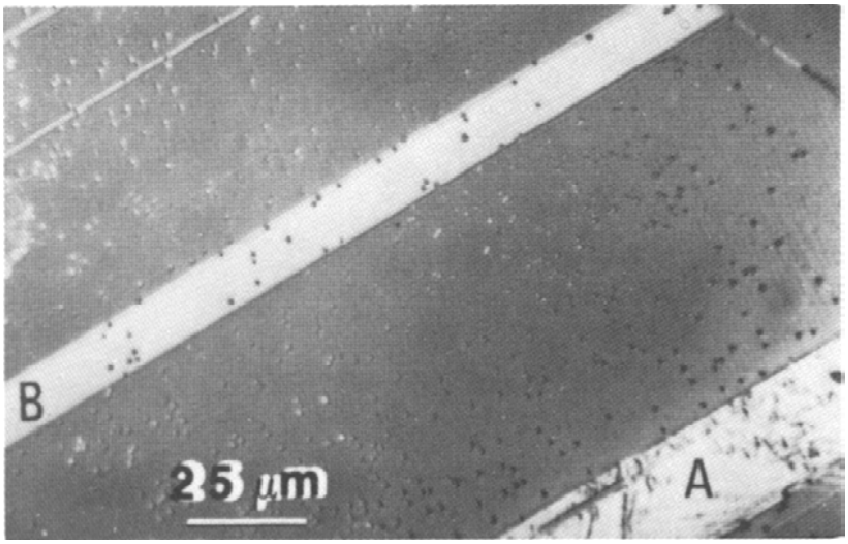

Figure 1-6 Martensites with band morphology under optical microscopy[10]

Generally, martensite has three forms of morphologies: lenticular plates, laths, and banded as shown through Figure 1-4 to Figure 1-6[10]. In most cases, martensites take the form of lenticular plates because this morphology comes from mechanical twinning, which has very low strain energy. In some low-carbon steels (up to 0.4 wt.% C), lath morphology can be observed. Unlike martensite in the form of lenticular plates, it is reported that the martensites in lath form are usually untwined as shown in Figure 5 [10]. The last morphology is the banded morphology. It can be observed in Fe-Mn-C alloys and shown in figure 6 [10]. In this case, the transformation takes place from FCC-HCP instead of FCC-BCC which happens in the previous two morphologies.

Martensitic transformation is a diffusionless transformation which can take place even at extremely low temperature. To have a clear understanding on martensite transformation, two ways can be used. Crystallographically, three phenomenological steps can be used to describe martensitic transformation: Bain strain, rigid body rotation and an inhomogeneous shear deformation. Bain strain can be understood as a homogeneous lattice distortion. It was first suggested by E.C.Bain [11] that martensitic transformation can be explained by a homogeneous “upsetting” of the parent fcc lattice into the required bcc (or bct) lattice, as shown in Figure 1-7 [12]. During deformation, the initial unit cell is contracted in one direction and extended in the other two orthogonal directions.

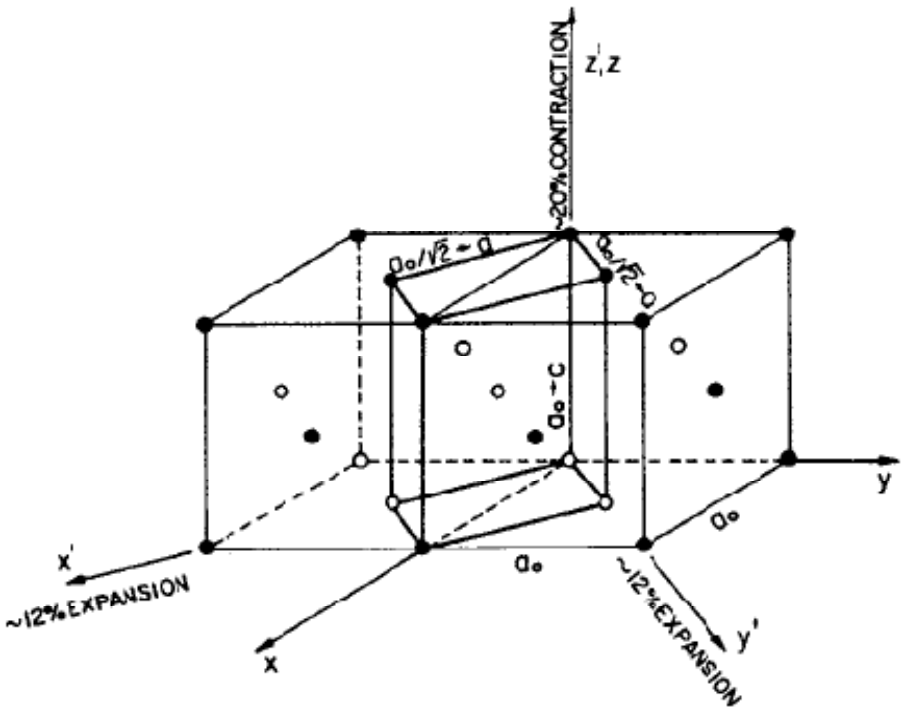

Figure 1-7 Schematic picture of Bain strain from FCC to BCC structure[12]

It is well established that the martensitic transformation is an invariant-plane transformation. More specifically, there should be an invariant plane (also known as the habit plane) on which no deformation takes place during transformation. By means of Bain strain alone, it is not possible to find an invariant plane. Furthermore, the lattice correspondence, which is a unique relationship between any lattice point in the initial lattice and the point it becomes in the final lattice, does not restrictively fulfill by a single lattice distortion. To fulfill the lattice correspondence, a rigid body rotation is introduced. This combined deformation is also known as the lattice deformation. However, even with the rigid body rotation, only an invariant-line strain could be guaranteed. In order to keep an invariant plane, an inhomogeneous shear deformation is further required. Such an inhomogeneous shear can be schematically shown in Figure 1-8. The dash lines indicate the twin boundaries involving internal twins after the

inhomogeneous shear. The function of this deformation is to change the shape without a structure change.

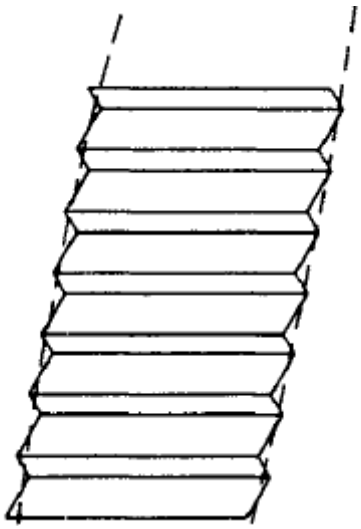

Figure 1-8 Schematic picture of the inhomogeneous shear involving internal twins[4]

Energetically, martensitic transformation can be also classified as either non-thermoelastic or theromelastic. Figure 1-9 shows the electrical resistance change during heating and cooling for non-thermoelastic (Fe-Ni) and thermoelastic martensitic transformation (Au-Cd) [4]. Apparently, non-thermoelastic martensitic transformation has a larger thermal hysteresis than thermoelastic transformation, indicating much larger energy dissipation during phase transformation. The reason behind such a big difference lies mainly on the interface between austenite and martensite. In thermoelastic transformation, the interface is partially or completely glissile, which means that the backward motion of interface is possible during reverse transformation and the martensite phase could grow fast after nucleation from the interface. On the other hand, in non-thermoelastic martensite transformation, the interface is not glissile and is immobilized during transformation. As a result of that, the nucleation of martensite has to happen in the austenite phase during forward transformation and the nucleation of

austenite should take place in martensite during reverse transformation. Furthermore, the martensite phase will not grow after nucleation upon cooling. Instead, multiple martensite phase fronts will nucleate throughout the parent phase, which in turns cause more energy and lead to more dissipation.

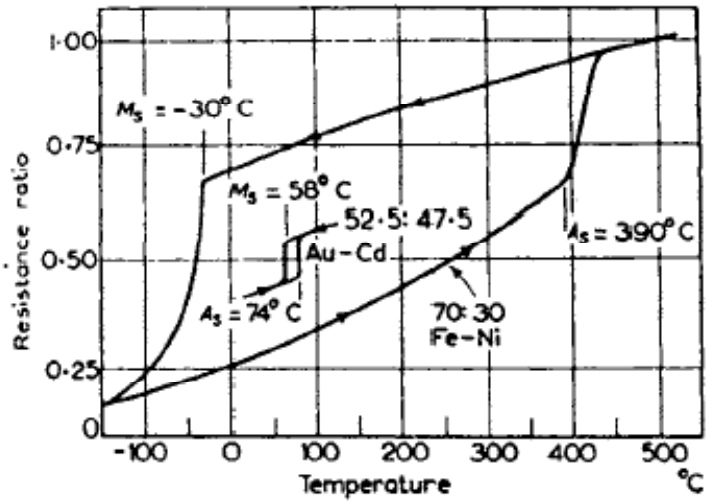

Figure 1-9 Electrical resistance evolution as a function of temperature for thermoelastic (Au-Cd) and non-thermoelastic (Fe-Ni) martensite transformation[4]

Regardless of whether it is thermoelastic or non-thermoelastic transformation, free energy change can be used to measure the energy required for martensitic transformation and predict if the transformation is going to take place based on the following,

$$\Delta G^{P-M} = \Delta G_C^{P-M} + \Delta G_{NC}^{P-M} \quad 1\text{-}1$$

where ΔG_C^{P-M} is the chemical free energy change and ΔG_{NC}^{P-M} is the non-chemical free energy change, including elastic stored energy, nucleation energy, mechanical energy and so on. The superscript P-M indicates the transformation from austenite to martenite. The change in chemical free energy could be schematically expressed using the difference between the free energy curves of the two phases, as shown in Figure 1-10. At temperature $T_{0,}$, both martensite and austenite have the same chemical free energy.

However, the martensitic transformation usually does not take place because of the non-chemical energy and dissipated energy. An overcooling is thus required to compensate for those energies in order for the transformation to take place. The transformation will be able to start if the total change of free energy is less than zero, as indicated by the condition at Ms in the figure.

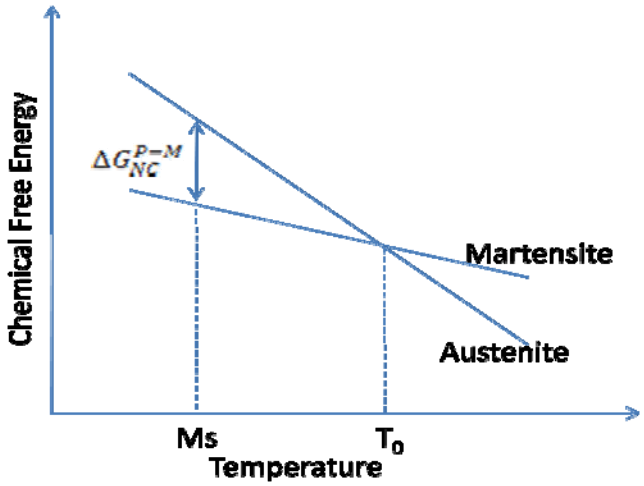

Figure 1-10 Relations between chemical free energy and temperature for martensite and austenite around martensitic phase transformation temperature[4]

Magnetic Shape Memory Alloys

Since 1996, ferromagnetic shape memory alloys (FMSMAs) have been studied as a new class of multifunctional materials that are capable of magnetic field induced actuation, sensing, magnetic refrigeration and energy-harvesting [4, 13, 14]. As a group of SMAs, MSMAs inherit the properties from conventional SMAs, e.g. shape memory effect [15, 16] and superelasticity [15, 16]. Furthermore, they also demonstrate unique magneto-mechanical coupling [17-19]. In other words, MSMAs are able to utilize magnetic field as another source of driving force for the reversible shape change. Since magnetic field can be cycled much faster than heat, MSMAs can be actuated much faster than conventional SMAs. Their actuation frequencies can reach kHz regime [20], as

indicated in Figure 1-11. Some MSMA products have already been developed in the past few years. One example is MSMA needle. Replacement of motor, gears and belts in a sewing machine with magnetically actuated MSMA needle can, to a large extent, simplify the structure of traditional sewing machines and thus reducing the cost of manufacturing. Two mechanisms are usually responsible for magnetic field induced strain (MFIS) in FMSMAs, which will be further discussed in the following sections.

Here, a brief review on the magnetic shape memory alloy system will be given. MFIS was first discovered by Ullakko *et al* [15] on off-stoichiometric Ni_2MnGa single crystal in 1996. Up to 10% MFIS was reported [21] on this material via field-induced martensite variant reorientation. However, brittleness and the low output stress (only about 5MPa) are two main problems for this material. To overcome these drawbacks, many alloy systems are developed, such as NiMnAl [22, 23], CoNiAl [24, 25], CoNiGa [26, 27] and NiFeGa [28]. The author's group characterized the magneto-thermo-mechanical properties of Ni_2MnGa [13], $Co_{49}Ni_{21}Ga_{30}$ [29, 30] and $CoNi_{33}Al_{29}$ [24, 25] alloys. For Ni_2MnGa, a reversible stress-assisted magnetic field induced transformation was first reported in 2006 [13, 14]. As for CoNiGa, reversible martensitic phase transformation is observed by changing in temperature, stress. A recoverable strain of 4% for compression was found [29, 30] for $Co_{49}Ni_{21}Ga_{30}$. Moreover, the precipitation of ductile γ phase at grain boundaries improves the ductility in polycrystalline $Co_{49}Ni_{21}Ga_{30}$, which cannot be achieved in Ni_2MnGa. CoNiAl was also verified as a promising shape memory alloys. As much as 4% strain in compression was reported accompanied with low stress hysteresis of about 40 MPa for [001] oriented $CoNi_{31}Al_{27}$ single crystals[25].

First developed by Kainuma et al, NiMnCoIn has been proved as a promising meta-magnetic SMA in recent years for actuator applications [31]. FIPT is the mechanism for MFIS in this case. The word "meta" here indicates that a magnetic phase transition happens accompany with the martensitic transformation. It was found that, the actuation stress of $Ni_{45}Mn_{36.5}Co_5In_{13.5}$ can be drastically increased up to above 100 MPa [32] through FIPT. However, the magnetic field required for FIPT is relatively high

which impedes the application of meta-magnetic SMAs. For the sake of practical application, it is important to characterize the magnetic properties of NiMnCoIn alloy in terms of magnetostress and to understand the effect of microstructures on the magneto-thermo-mechanical behavior of this material.

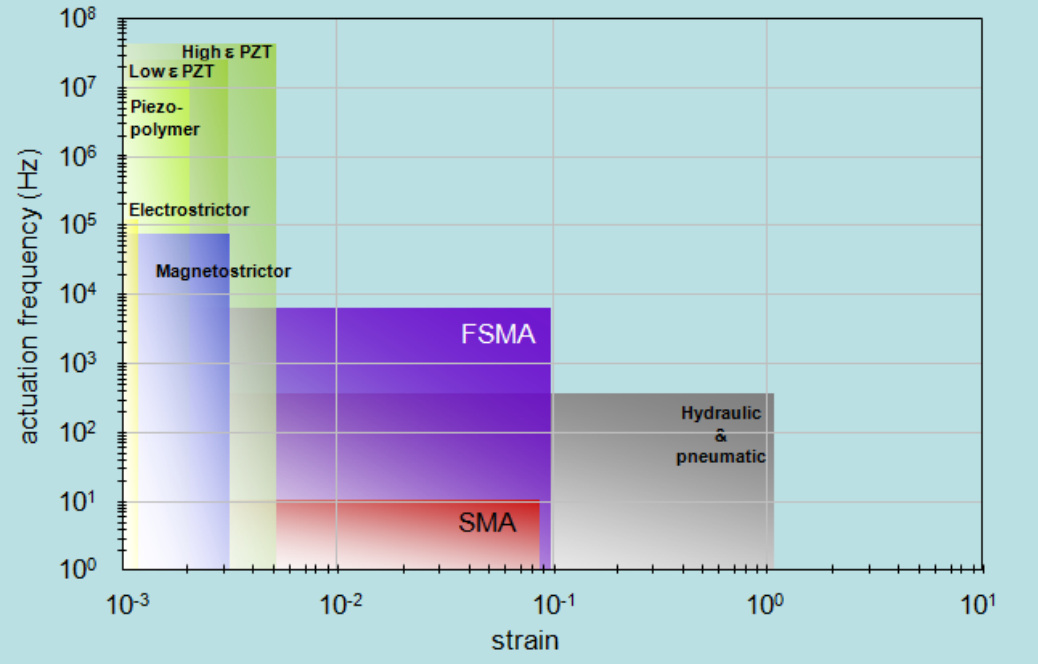

Figure 1-11 Comparison of the actuation frequencies and actuation strains of various smart materials including ferromagnetic shape memory alloys

Magnetic Field Induced Martensite Variant Reorientation

The first mechanism responsible for MFIS is field induced martensite variant reorientation [13]. Crystallographically, martensitic transformation is a diffusionless transformation from a high symmetric phase (austenite) to a low symmetric phase (martensite). In this case, a number of martensites with different habit plane (martensite/austenite interface) indices but equivalent in crystallography [16] can be generated throughout the material during transformation, which is known as martensite

variants. In order to minimize the energy upon transformation, these variants are usually twin related and tend to self-accommodate each other to keep the shape unchanged under stress and magnetic field free condition. In FMSMAs, magnetic momentums tend to alien towards certain direction without magnetic field. This direction is called the easy axis of magnetization. When an external magnetic field is applied, these momentums are likely to rotate to another axis, which is known as the hard axis of magnetization. Martensite variants reorient with such rotation of magnetization axis. As a result, twin boundaries will move and one variant grows up at the expense of the others accompany with the martensite variants reorientation, as shown in Figure 1-12. The field-induced boundary motion here is the reason for the MFIS. Magnetocrystalline anisotropy energy (MAE) is the driving force responsible for the MFIS. It can be described as the area between the easy axis and hard axis in the M-H curve (magnetization versus magnetic field), as shown by the shaded area in Figure 1-13. It is also a measurement of how much energy is required to rotate the direction of magnetization from hard magnetization axis to easy magnetization axis. In order to obtain MFIS, MAE energy should be larger than the energy required for twin boundary motion. If MAE is smaller than the energy required for twin boundary motion, the external magnetic field will rotate the magnetization axis towards the applied field direction. However, since the weak MAE could only provide limited pressure on the twin boundary, the twin boundary will not move. As a result, no MFIS can be obtained. On the other hand, if MAE is high, MFIS can be realized through the twin boundary motion and redistribution of different twin variant fractions under magnetic field [33].

As introduced above, MAE can be expressed as the area between the M-H response of the easy axis and hard axis. There are only two ways to increase this area and thus the available magnetic energy to be converted into mechanical output as shown in Figure 1-14. The first way is to increase the critical magnetic field for the hard axis. Here, the critical magnetic field for the hard axis means the minimum magnetic field required to reach the saturation magnetization when the magnetization of the material is saturated along hard axis of magnetization, as indicated by H^{c}_{hard} in Figure 1-14.

However, a limited area change can be achieved by this method because the saturation magnetization level (the magnetization level for the plateau of the curve) does not change. Second, this area can also be increased by shifting the plateau up, in other words, by increasing the saturation magnetization of martensite. This can be attained by increasing the Curie temperature or by decreasing the operating temperature. Generally, the saturation magnetization of magnetic material gets higher when the operating temperature is getting lower from Curie temperature.

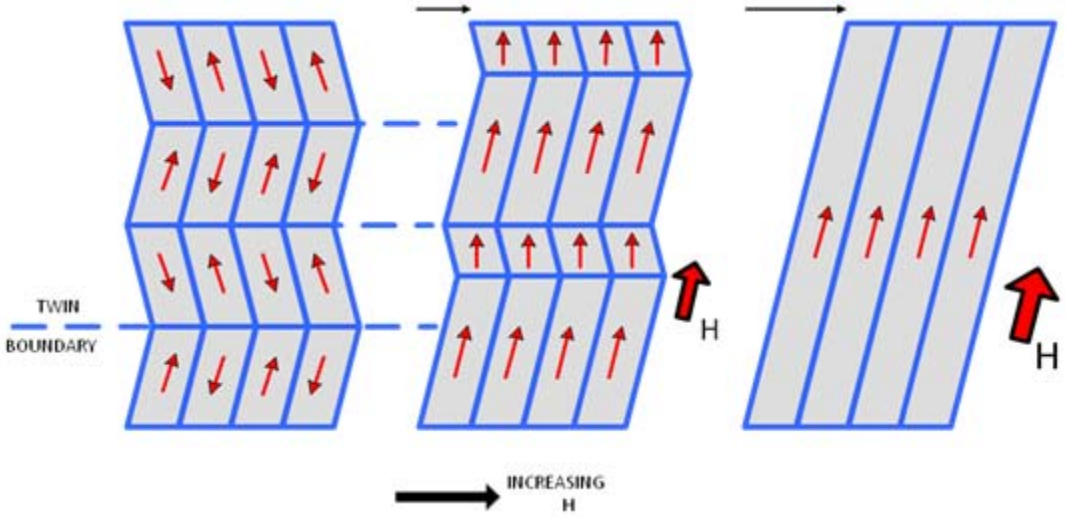

Figure 1-12 A schematic showing the growth of one martensite variant at the expense of the other in a two variant system under magnetic field

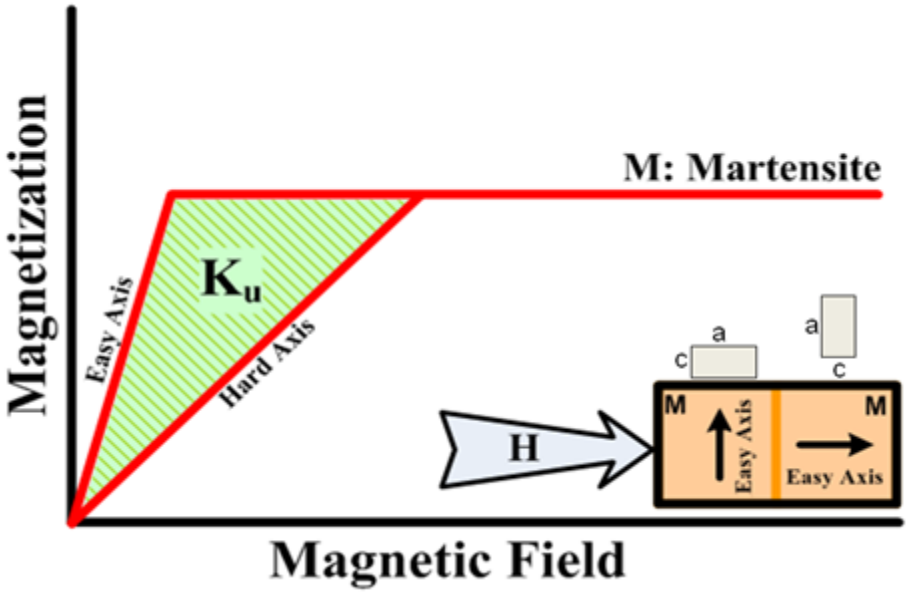

Figure 1-13 Schematic magnetization versus magnetic field curve, MAE is expressed by the area surrounded by M-H curve of easy axis and hard axis

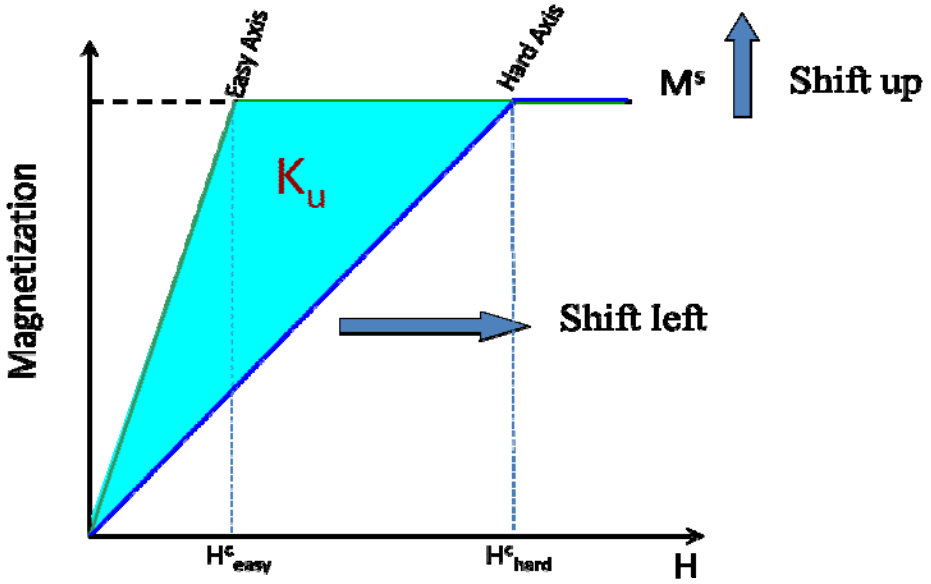

Figure 1-14 Two ways for increasing MAE: increasing critical magnetic field for the hard axis of magnetization, or increasing the saturation magnetization of martensite

Magnetic Field Induced Phase Transformation

The second mechanism responsible for MFIS is field-induced martensitic phase transformation (FIPT). Some off-stoichiometric Ni_2MnZ (Z=In, Sn, Sb) Heusler alloys with B2 or $L2_1$ crystal structures were reported to exhibit ferromagnetism in austenite and antiferromagnetism (paramagnetism) in low temperature martensite phase [34-37]. As shown in Figure 1-15 [38] for $Ni_{50}Mn_{34}In_{16}$, when cooled down from high temperature under external magnetic field, the material first experiences a second order phase transition from paramagnetic austenite to ferromagnetic austenite at Curie temperature around 260 K. Further cooling leads to a first order martensite transformation, in which magnetization of the material drastically decreases to a very low level, indicating a magnetic phase transition from ferromagnetic austenite to paramagnetic (or antiferromagnetic) martensite [38]. Recently, Umestu *et al* [39] performed Mossbauer spectroscopy study on the martensite of $Ni_{50}Mn_{36.5}{}^{57}Fe_{0.5}Sn_{13}$ and proved that the material is paramagnetic in martensite phase. It is believed that the martensite of NiMnIn alloy should also shows paramagnetism. The magnetic status for each temperature stage is schematically shown in the upper part of Figure 1-15. The arrows indicate the direction of magnetic moment between atoms in a unit cell. The drastic change in magnetization during martensite transformation provides a significant Zeeman Energy difference which is energy responsible for FIPT, and thus MFIS.

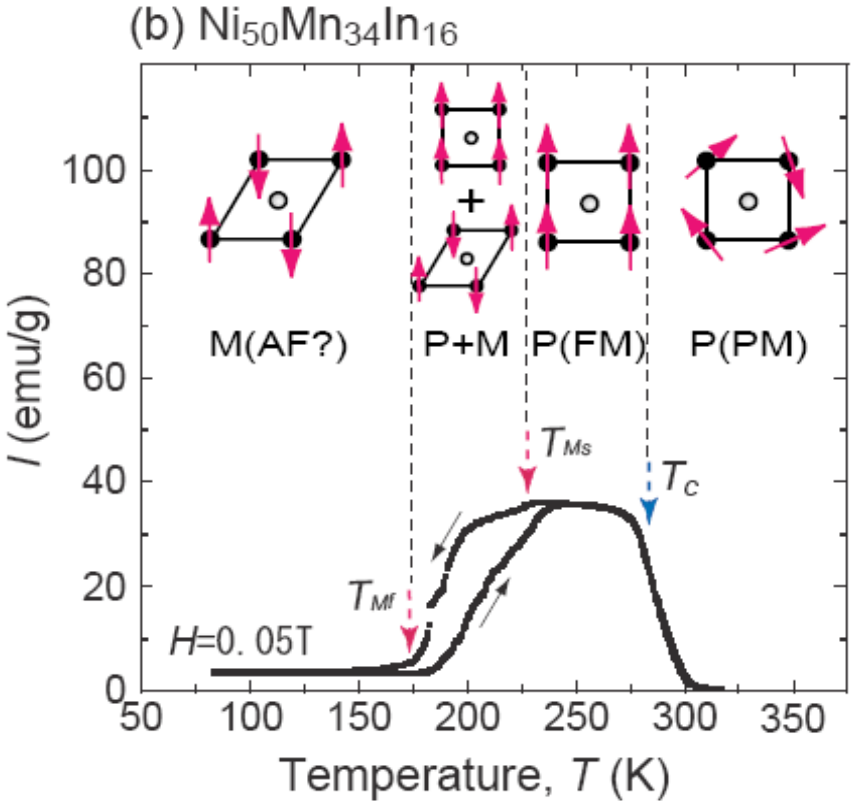

Figure 1-15 Isothermomagnetization curve for $Ni_{50}Mn_{34}In_{16}$ from SQUID shows the martensite transformation with changing temperature. The upper part is the schematics of the crystallographic structure and magnetic phase of the material[38]

Compared with the field-induced martensite variant reorientation, this mechanism has two main advantages. First, the driving force is large. Zeeman Energy is the driving force FIPT, as mentioned above. As is schematically shown using M-H curve in Figure 1-16, the martensite and austenite have different saturation magnetization in this case. The Zeeman Energy could be taken as the magnetic energy difference between martensite and austenite, as indicated by the area in Figure 1-16. This Zeemen Energy increases linearly with applied magnetic field [14, 40] after quickly reaching the saturation in magnetization. In Figure 1-16, magnetization saturates at certain magnetic field for martensite and austenite phase followed by a big plateau. This indicates that the

energy could be increased linearly with magnetic field without an upper limit, theoretically. The second advantage is the giant entropy change. The magnetic form of Claussius-Clapeyron relation in the magnetic phase diagram can be expressed as follows,

$$\frac{dH}{dT} = -\frac{\Delta S}{\Delta M} \qquad 1-2$$

where H is the applied magnetic field, T is the temperature, S is the entropy and M is magnetization. Entropy change during martensite phase transformation can be calculated by integrating the following equation:

$$\Delta S(T,H) = \mu_0 \int_0^H \left(\frac{\partial M}{\partial T}\right)_H dH \qquad 1-3$$

From these equations, it is obvious that entropy change has a close relation to the change in magnetization with martensite transformation temperature under external magnetic field. More specifically, since martensite and austenite are in non-ferromagnetic and ferromagnetic or vice versa, the magnetization drastically changes with martensitc transformation. Moreover, magnetic field either energetically favors or unfavors the martensitic transformation, such that the transformation temperature varies with and without magnetic field. For alloys such as NiMnCoIn, the change in magnetization between austenite and martensite phase is usually large (about 100 emu/g), which leads to an entropy change of about 27 $JK^{-1}kg^{-1}$ [31]. The entropy change during martensite transformation under magnetic field is usually also known as magntocaloric effect (MCE). In recent years, many magnetic shape memory alloy systems are discovered to have giant magnetocaloric effect [31, 41, 42], some of which are summarized in Table 1-1.

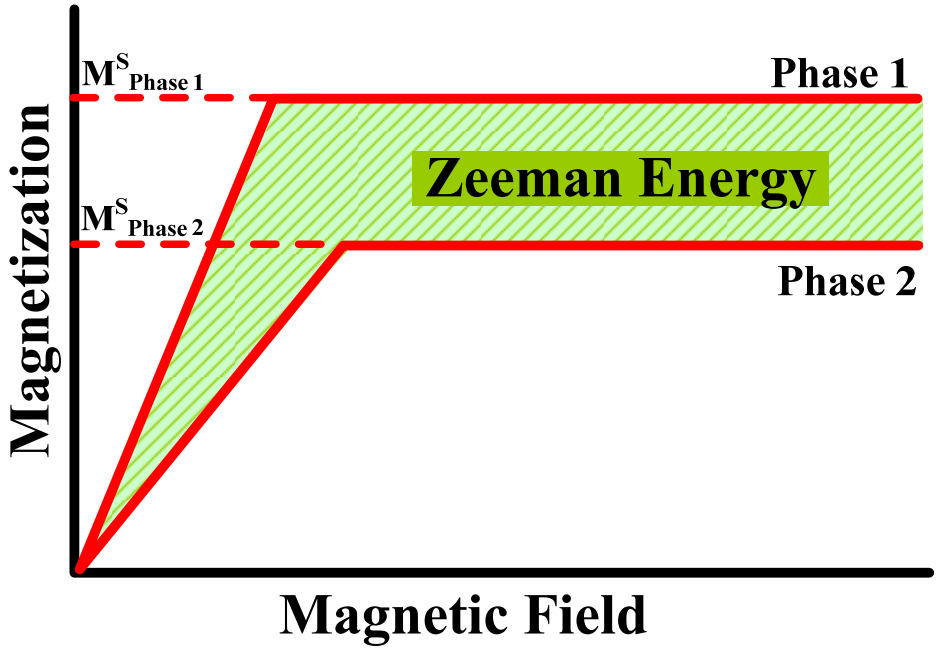

Figure 1-16 Schematic picture of Zeeman Energy difference in M-H curve. Martensite and austenite phase have different saturation magnetization level[32]

Table 1-1 Entropy change due to martensite transformation for some FMSMAs

Alloy	$\Delta S\ JK^{-1}kg^{-1}$[37, 43-47]
$Ni_{46}Mn_{41}In_{13}$	17.1
$Ni_{45}Co_5Mn_{36.7}In_{13.3}$	27
$Ni_{48.3}Mn_{36.1}In_{10.1}Sb_{5.5}$	21.5
$Ni_{50}Mn_{35}In_{14}Al$	10
$Ni_{50}Mn_{35}In_{14}Ge$	50
$Ni_{50}Mn_{35}In_{14}Si$	83
$Gd_5(SixGe1–x)_4$	20
$Ni_{0.50}Mn_{0.37}Sn_{0.13}$	18
$Ni_{48}Co_2Mn_{38}Sn_{12}$	37.2
$Mn_{1.96}Cr_{0.05}Sb$	7

Effect of Magnetic Field on the Superelastic Response of Magnetic Shape Memory Alloys

Figure 1-17 shows the stress-strain behavior of $Ni_{45}Mn_{36.5}Co_5In_{13.5}$ single crystals at a temperature above the reverse martensitic phase transformation finish temperature (A_f). The black curve exhibits the stress strain relation without magnetic field under compression. With applied stress, the material first deforms in the elastic region and strain increases linearly with increasing stress up to 0.4%. The material starts to transform into martensite phase when applied stress reaches the critical stress at about 120 MPa. At this stage, a stress increase much slower with increasing strain and this region is known as superelastic plateau. The stress-strain slope starts to increase again at about 2.1% strain level. When unloaded at 2.5% strain, stress-strain response shows similar trend as in loading expect for the hysteresis loop. When an external magnetic field (1.6T) is applied, the stress strain curve tends to move upwards, as the purple curve shown in the figure. The stress-strain slope in austenite region is about the same as the magnetic field free condition. However, the material starts to transform into martensite at a higher stress level. The corresponding superelastic plateau is thus moved upwards in the figure. The difference in compression stresses between two plateaus of the curves is defined as magnetostress. Magnetostress is caused by Zeeman energy difference between martensite and austenite phases due to the constant applied magnetic field. In $Ni_{45}Mn_{36.5}Co_5In_{13.5}$, magnetic field favors the formation of parent austenite phase. In this case, magnetostress can be considered as the extra applied barrier for martensitic transformation due to the external magnetic field.

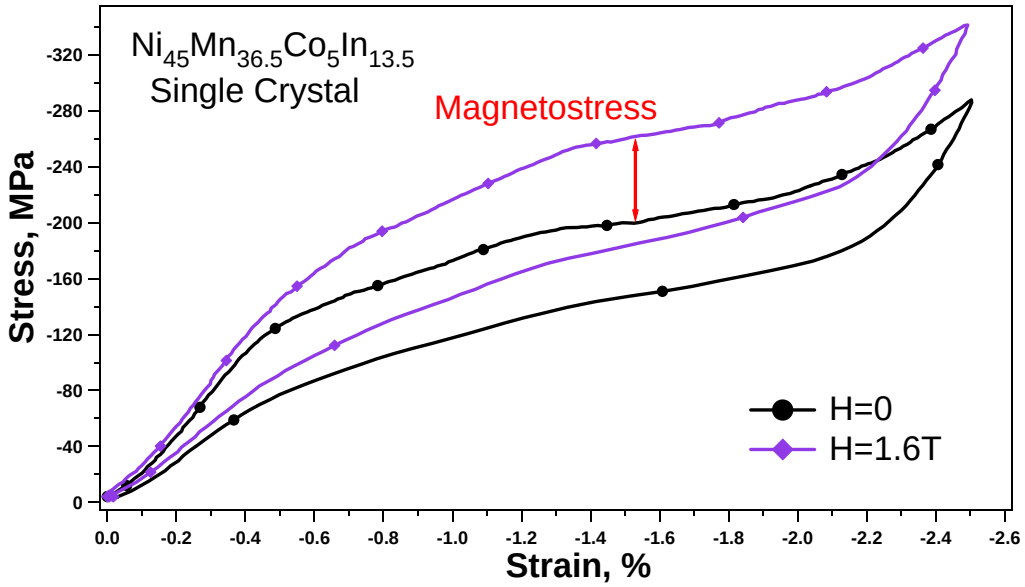

Figure 1-17 Stress-strain curve for $Ni_{45}Mn_{36.5}Co_5In_{13.5}$ single crystal with and without magnetic field. Magnetostress is indicated by the red arrow in the figure

Metamagnetic Shape Memory Effect

Figure 1-18 shows the strain-magnetic field response for $Ni_{45}Mn_{36.7}Co_5In_{13.3}$ single crystals. A pre-strain of approximately 3% was initially applied along compressive direction without magnetic field at 298K. The material is in martensite phase at the temperature. When an external magnetic field is applied vertically to the compressive axis of the specimen, the recovery strain started to increase at 2 Tesla and drastically recovered at about 3.6 Tesla. The magnetic field was loaded up to 8 Tesla and the maximum recovery strain was about 2.9%. This is so called metamagnetic shape memory effect. The drastic change in strain level at 3.6 Tesla is because of the reverse martensitic transformation induced by magnetic field. Kainuma *et al* observed this effect on $Ni_{45}Mn_{36.7}Co_5In_{13.3}$ [38]. Similar phenomenon was also reported for NiMnCoSn [48].

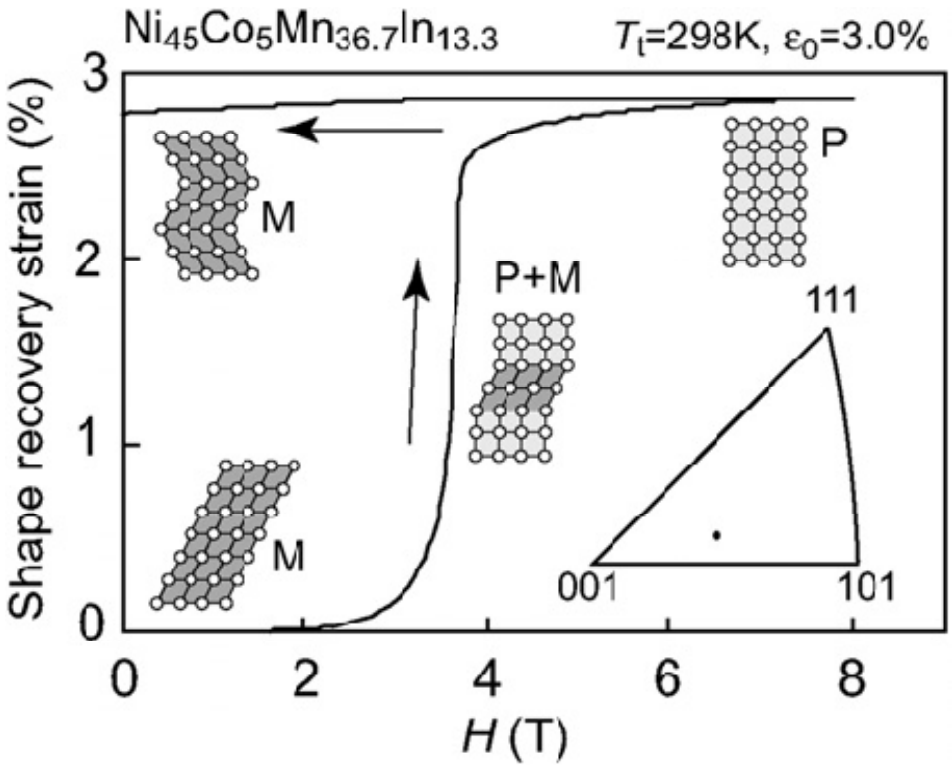

Figure 1-18 Metamagnetic shape memory effect in $Ni_{45}Co_5Mn_{36.7}In_{13.3.}$ Shape strain recovers with the increasing magnetic field. A drastic strain change takes place at 3.6T due to the reverse field induced martensitic transformation[38]

Stress-assisted Reversible Magnetic Field Induced Phase Transformation

As mentioned in the previous section, retained compressive strain can be recovered under magnetic field. In the example of $Ni_{45}Co_5Mn_{36.7}In_{13.3}$ above, magnetic field transforms the detwinned martensite into austenite and upon unloading the field, the material transforms back to self accommodated martensite. Unfortunately, the recovered strain cannot return to the initial level when the magnetic field is unloaded since the material is not trained. More important, the magnetic field required to induce reverse martensitic transformation is very high (3.6T), which is not possible for practical application. To reduce the magnetic field required for such reverse martensitic transformation, stress is introduced to take the place of part of magnetic energy required

for back transformation. To explain how stress-assisted reversible magnetic field induced phase transformation works, Figure 1-19 is shown schematically containing the superelastic behavior with and without magnetic field. Assuming the operating temperature is above A_f, the stress is applied without magnetic field to transform the material into martensite phase and unloaded to a stress level which is slightly higher than the critical stress for martensitic transformation. The reason of keep the load at such level is to minimize the magnetic field required for reverse transformation. When magnetic field is applied, the material is transforming back into austenite because the critical stress for martensite transformation increases and the held stress is not large enough to keep the material in the martensite phase under magnetic field, thus recovering the strain. When magnetic field is removed, the held stress is again large enough for transform the material into martensite phase, such that the strain increases with the martensitc transformation.

However, such “reversible” stress-assisted field induced martensitic phase transformation has an important prerequisite. That is, the superelastic loop with and without magnetic field should be separated. In other words, the magnetostress must be higher than the stress hysteresis. Here the stress hysteresis is defined by the critical stress difference between forward and reverse martensitic transformation. More specific, the magnetic energy imported must be larger than the energy dissipated during martensitic transformation. To rationalize that, Figure 1-20 is shown in which the two loops are not separated. In this case, if the same procedure is repeated, it is found that when magnetic field is applied, the martensitic transformation is not likely to happen because the held stress is still higher than the critical stress for the transformation and the material remains in austenite phase.

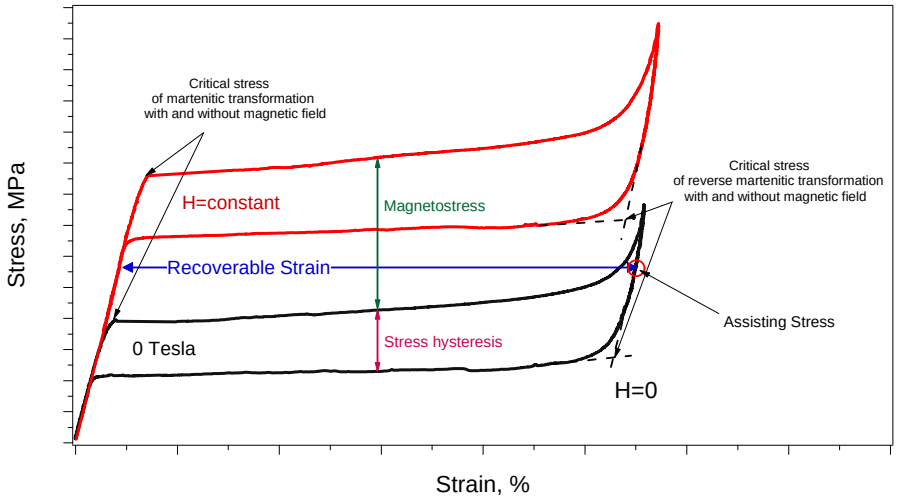

Figure 1-19 A schematic of stress-assisted reversible martensitic phase transformation. The red curve and black curve shows the superelastic behavior of a FMSMA with and without magnetic field at temperature above A_f. Assisting stress is held at a level in between the critical stress of martensitic transformation under zero field and the critical stress of reverse martensite transformation under magnetic field. Recoverable strain indicates the strain recovered after loading magnetic field

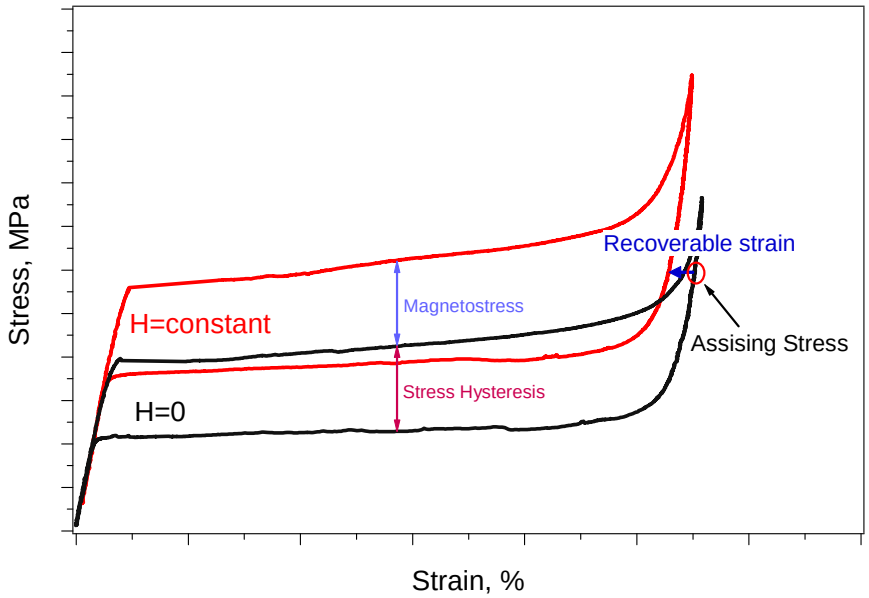

Figure 1-20 A schematic picture shows the recoverable strain if the two superelastic loops are not separated. Recoverable strain is very limit because the assisting stress is higher than the critical stress of reverse martensitic transformation

Transformation Hysteresis in SMAs

Martensitic transformation can be induced reversibly by temperature, stress, or magnetic field with an accompanying transformation hysteresis. Transformation hysteresis indicates the energy dissipated during both forward and reverse martensitic transformation. A lot of effort has been made in the past years to reveal the origin of hysteresis [49-51]. In general, the main mechanisms for transformation hysteresis during martensitic transformation are lattice friction, defect generation and transformation induced plasticity. Dislocations can be generated during martensitic transformation [52] and the interaction between the interfaces and defects leads to energy dissipation. Transformation induced plasticity is important to understand for microstructure design to reduce transformation induced hysteresis, because it describes how hard it is for the matrix to accommodate the martensite volume change and transformation shear and thus reflect the compatibility between austenite and martensite phases. The hysteresis can be influenced by several factors. Thermal and mechanical history can also greatly contribute to the hysteresis, such as thermo-mechanical cycling and aging in martensite. Furthermore, the level of ordering in the parent phase, heating-cooling rate, and loading rate are all possible factors to affecting the hysteresis.

Cobalt Based Shape Memory Alloys

As is mentioned above, many factors can influence the hysteresis. But some of the factors, e.g. transformation plasticity, could be more or less controlled by changing the compatibility conditions of the material, which is feasible through alloy or microstructure design. CoNiAl is a promising shape memory alloy with a recoverable compressive strain up to 4% [24, 53]. Moreover, this alloy processes a very high strength and good ductility. It is reported that both thermal and stress hysteresis of this material decreases with increasing stress and temperature, respectively [25]. By working on this material, it is beneficial to understand the relation between compatibility mentioned above and the hysteresis.

In addition, the loading conditions influence the mechanical behavior of

ferromagnetisms. Specifically, transformation strain changes with temperature and trends are material and microstructure dependent [25, 29, 54-57]. It have been reported that the transformation strain slightly increases with increasing temperature in NiTi alloy [57]. However, it decreases with temperature in CoNiAl [25] and NiFeGa [55]. Moreover, such anomaly in transformation strain is single crystal orientation or crystallographic texture dependent. Unfortunately, the mechanisms that are responsible for such anomaly are also not clear. However, the knowledge of these responsible mechanisms is extremely important for engineering. Therefore, one of the goals of this thesis research is to reveal the aforementioned anomaly on the temperature dependence of transformation strain through working on CoNiAl alloy.

Objective of the Work

As mentioned above, NiMnCoIn single crystal has been proved to be a promising meta-magnetic shape memory alloy which shows a magnetic output work of more than 1MJ/Tesla. Since the austenite of the material shows ferromagnetic while martensite shows paramagnetic, shape change of the NiMnCoIn could be performed using magnetic field-induced martensitic transformation. However, the magnetic field required for martensitic transformation in this case is too high for practical application (3~5T). Stress could be introduced to reduce the magnetic field required for magnetic field induced transformation. Yet no literature has reported the magnetic field required for stress-assisted reversible field induced martensitic transformation on that material. The ultimate goal of the work in the long term is to achieve such reversible martensitic transformation at a magnetic field as low as possible.

To achieve the magnetic output work, magnetic energy imported by external magnetic field must be larger than the energy dissipated during actuation such that the rest part of magnetic energy could be converted to mechanical energy and thus be utilized for actuation. This means, the superelastic loops of the material with and without magnetic field must be separated as shown in Figure 1-20. In other words, the magnetostress should be larger than the stress hysteresis. Not considering the change of transformation strain and stress hysteresis, magnetostress is very essential to realize the stress-assisted magnetic field induced martensitic transformation.

So, the main objective of the current work is to examine the effect of temperature, heat treatment and orientation on the magnetostress in $Ni_{45}Mn_{36.5}Co_5In_{13.5}$ meta-magnetic shape memory alloys.

On the other hand, transformation strain and hysteresis changes under different temperature and applied stress. Furthermore, there is an “anomaly” for different materials in the change of transformation strain as function of temperature or applied stress. It is important to know where such anomaly comes from.

Thus, the second objective is to understand the thermo-mechanical loading conditions on the phase transformation of FMSMAs. $Co_{48}Ni_{33}Al_{29}$ single crystal with [001] orientation, was selected in this study because of its high strength. [001] orientation was picked due to the lack for slip system along that direction, thus the dislocation is hard to form and the strength of the material would be better than other orientations.

CHAPTER II
EXPERIMENTAL PROCEDURES

The ingots of both $Ni_{45}Mn_{36.5}Co_5In_{13.5}$ and $CoNi_{33}Al_{29}$ alloys were prepared using vacuum induction melting. Single crystals were grown using the Bridgman technique in He atmosphere. The crystals were then cut into rectangular prism shape samples with the dimensions of 4 mm x 4mm x 8mm using wire electro discharge machining. The long axes of these samples were used as the compression axis. In austenite phase, the compression axes were along [100] and [111] directions.

The magneto-thermo-mechanical behavior of the crystals was determined using a custom built Magneto-Thermo-Mechanical setup upon a MTS servohydraulic mechanical test frame. A Lake Shore Model EM4-CS electromagnet was employed to generate a uniform magnetic field up to 1.6 Tesla. Custom-built nonmagnetic Ti-6Al-4V alloy grips were attached to the test frame. A Lake Shore high sensitivity cryogenic transverse Hall probe sensor (with a resolution of ±0.01 mT within the ±30 T range) was combined within a Lake Shore model 450 gaussmeter to measure the magnetic field during the tests. The probe was placed perpendicular to the compression axis. A capacitive displacement sensor (Capacitec, Ayer, MA, USA) was used to measure the strain. Heating and cooling was controlled by an Omega CN8200 series temperature controller for each grip. Copper tube was wrapped around the grips and liquid nitrogen was run though it to cool down the grips. A cryogenic grade, on/off solenoid valve connected to temperature controller was used to control the flow of liquid nitrogen. Heating was achieved by the heating band wrapped around the tubes. To keep a constant volume during the tests, a non-magnetic polymer chamber was fabricated and placed in between the electromagnet pole pieces.

For the NiMnCoIn single crystal work, all the samples were homogenized at 900°C for 24 hours. Furnace cooling, water quenching, and oil quenching were used after homogenization for the [001] orientated samples. Furnace cooling and water quenching were conducted on the [111] orientated samples. It is worth mentioning that a

slight difference of composition may exist among the samples we use in this study after heat treatment at 900°C because of the low melting temperature of In element (Ms decreases 18K for 0.1% drop in In [58]). Since In affects the transformation temperature for the material, the transformation temperature we determine in the study may not be able to reflect the exact transformation temperature on $Ni_{45}Mn_{36.5}Co_5In_{13.5}$.

To understand the effect of orientation and heat treatment on the phase transformation characteristics, heating-cooling and pseudoelastic experiments were conducted for all specimens. Critical transformation temperatures, transformation strains and stresses were recorded such that stress-temperature phase diagram could be constructed to reveal the effect of structural change due to different cooling rate on phase transformation behavior.

Pseudoelastic experiments were conducted under constant magnetic fields in the range of 0 T to 1.6 T at various temperatures for [001] and [111] oriented specimens to reveal the effect of magnetic field on the thermo-mechanical behavior.

To better understand how microstructure changes with the cooling rate, the samples were examined using a high-energy XRD at the 11-ID-C beam line at the Advanced Photon Source, Argonne National Laboratory, USA with a wavelength of λ=0.010756 nm.

The magnetic properties were determined using a Quantum Design Superconducting Interference Device magnetometer. The samples were cut into small pieces with the weight on the order of milligrams before testing. Thermomagnetization experiments, in which magnetization changes with temperature, were conducted under 0.05 T and 7 T to find out the magnetic properties of in high temperature austenite and low temperature martensite phases. In addition, this set of experiments is helpful to determine the effect of magnetic field on the structure phase transformation. Magnetization experiments were conducted on the specimens in the vicinity of martensite transformation temperature to explore the relation between magnetization and magnetic field and to observe field-induced phase transformation if exists.

Table 2-1 lists the experiments conducted in this study for $Ni_{45}Mn_{36.5}Co_5In_{13.5}$

single crystals.

Table 2-1 Experiments performed on $Ni_{45}Mn_{36.5}Co_5In_{13.5}$ to examine the effect of orientation, heat treatment and temperature on the magnetostress of the material

	Isobaric thermal cycling tests	Pseudoelastic tests with and without magnetic field	X-Ray diffraction	SQUID magnetometer
Heat Treatment Effect	On furnace cooled, water quenched and oil quenched samples with [001] orientation	On furnace cooled, water quenched and oil quenched samples at magnetic field from 0T to 1.6T with [001] orientation	On furnace cooled, water quenched and oil quenched samples with [001] orientation	At 0.05T and 7T for furnace cooled, oil quenched and water quenched samples with [001] orientation
Orientation Effect		On furnace cooled sample with [001] and [111] orientations from 0T to 1.6T		
Temperature Effect		At 0T and 1.6T on furnace cooled sample material with [001] orientation		At 0.05T and 7T for furnace cooled, oil quenched samples with [001] orientation

$CoNi_{33}Al_{29}$ single crystals were homogenized at 1325°C followed by water quenching. To examine the effect of loading conditions on the thermo-mechanical behavior of these crystals, heating-cooling experiments were conducted at various temperatures under constant stress levels ranging from 10 MPa to 200 MPa. Pseudoelastic experiments were performed at temperatures between 35°C and 175°C. A test matrix is also given as follows.

Table 2-2 Experiments performed on $CoNi_{33}Al_{29}$ single crystal to examine the effect of loading conditions on the thermo-mechanical behavior of these crystals

	Stress (MPa)	Temperature (°C)
Isobaric thermal cycling experiments	N/A	35, 55, 75,95,115,135,155,175
Pseudoelastic experiments	25, 50, 100, 150, 200	N/A

CHAPTER III
THE EFFECT OF CRYSTAL ORIENTATION, TEMPERATURE AND COOLING RATE ON THE MAGNETO-THERMO-MECHANICAL RESPONSE OF NiMnCoIn META-MAGNETIC SHAPE MEMORY ALLOYS

Isobaric Thermal Cycling and Superelastic Experiments on $Ni_{45}Mn_{36.5}Co_5In_{13.5}$ Metamagnetic Shape Memory Alloys

The thermo-mechancial tests were conducted furnace cooled, oil quenched and water quenched samples oriented along [001] and [111] directions. Isobaric thermal cycling and pseudoelastic tests results are shown below.

Figure 3-1a shows the isobaric thermal cycling test result from $Ni_{45}Mn_{36.5}Co_5In_{13.5}$ after homogenized at 900°C for 24 hours and furnace cooled.

The specimen was first heated-cooled under 50 MPa in the temperature range from -90°C (183K) to 80°C (193K), as shown by the black loop in the figure. Afterwards, another cycle under 75 MPa was preferred in the same temperature region as shown by the purple loop. The martensitic transformation start temperature (Ms) is defined by the temperature value of the intersection of two tangent lines, as indicated in the figure. Obviously, the Ms temperature increased with applied external stress. From equation 1-1, when stress increases, more mechanical energy is applied to the system which to some extent replaces the energy from undercooling so that the phase transformation takes place at a higher temperature. Furthermore, it is observed that the compressive transformation strain increased with external stress. It is well established that martensite variants tend to self-accommodate in stress free condition to minimize the energy required for transformation [4]. External stress functions as the bias stress to form one favored variant at the expense of the others. In other words, the larger the external force, the more volume of martensite variants is biased, which in turn leads to a larger observed transformation strain. However, this strain could not be increased above the theoretical transformation strain. Compressive strain saturates when all variants are

biased into one. Finally, there are some temperature jumps during heating and cooling period in both loops. It is believed that this comes from experiment errors.

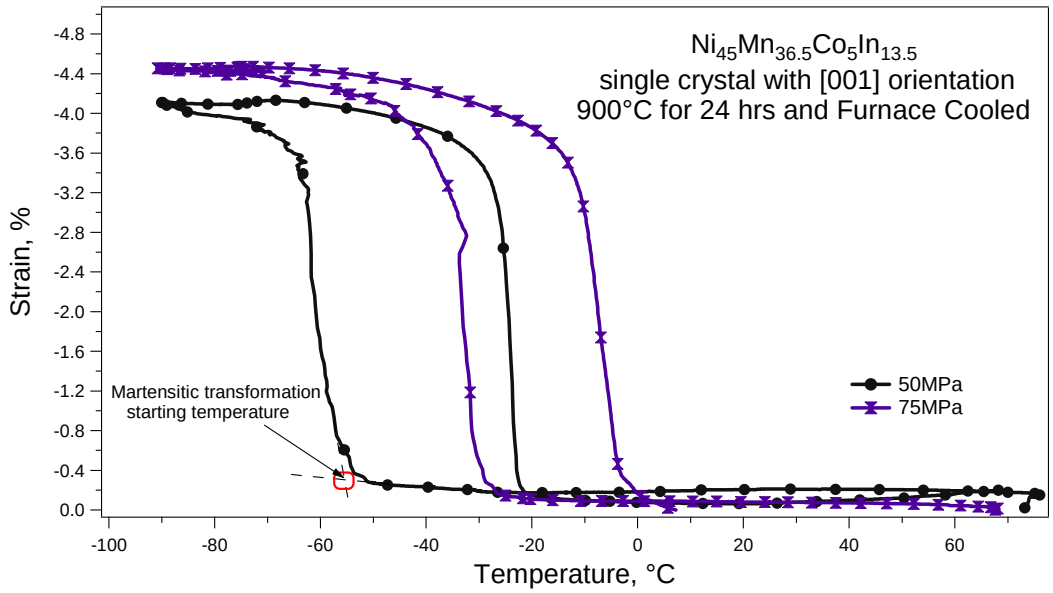

Figure 3-1a Isobaric thermal cycling test for furnace cooled $Ni_{45}Mn_{36.5}Co_5In_{13.5}$ with [001] orientation under 50 MPa and 75 MPa

Figure 3-1b shows the pseudoelastic behavior for the furnace cooled sample at various temperatures. The sample was tested in the temperature range from 228K to 293K. The critical stress, which indicates the martensite transformation start point, is determined from the intersection of two black lines in the figure. Analogous to isobaric thermal cycling behavior, the critical stress also increases with temperature.

Similar experiments were conducted on water quenched and oil quenched samples with the [001] orientation. Also, furnace cooled and water quenched samples with the [111] orientation were tested. Moreover, in order to make sure that the thermo-mechanical testing results are repeatable, the same experiments were conducted on different samples with exactly same orientation and heat treatments.

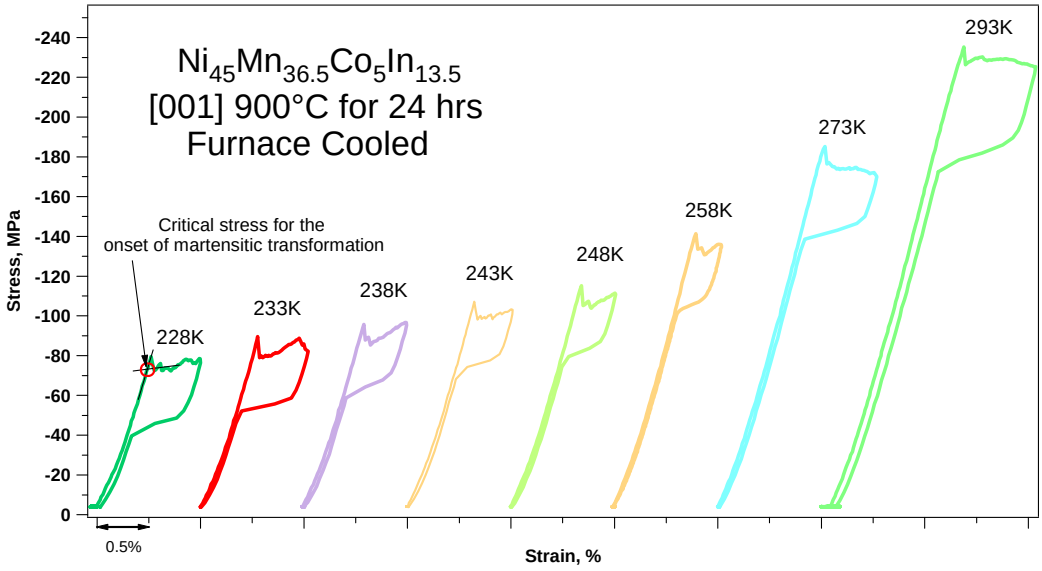

Figure 3-1b Superelastic stress versus strain response of $Ni_{45}Mn_{36.5}Co_5In_{13.5}$ single crystals oriented along the [001] direction under compression after furnace cooling from 900°C. The experiments were conducted at different temperatures

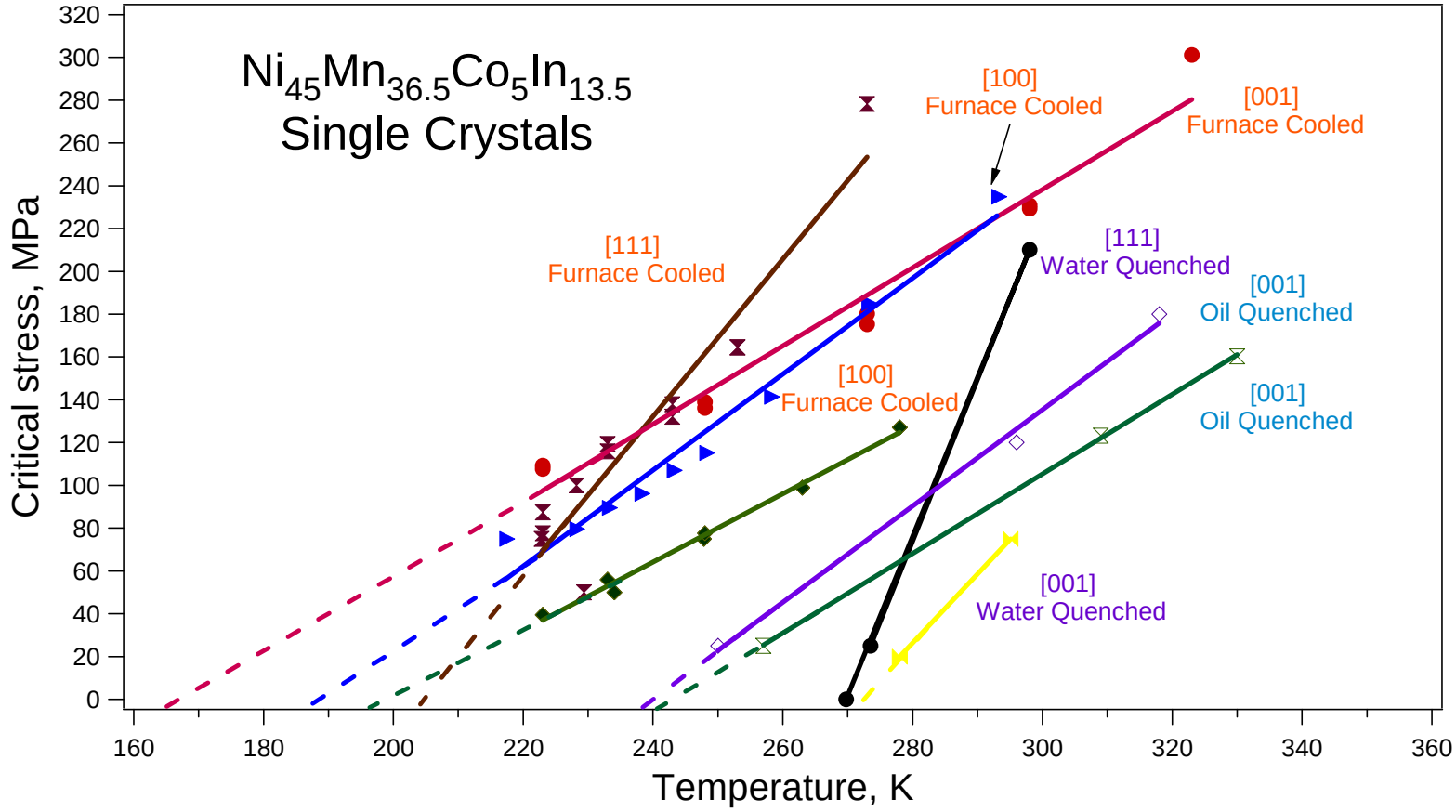

Figure 3-2 Critical stress versus temperature phase diagram of $Ni_{45}Mn_{36.5}Co_5In_{13.5}$ single crystals for martensitic transformation as a function of crystallographic orientation and cooling rate

Before further discussion, it is worth noting that there are notable differences between the samples of the same conditions. This is mainly because of the difficulty in achieving exactly same composition from one batch of single crystals to another and compositional inhomogenity in a given single crystal. These issues are common for all magnetic SMAs containing Mn due to the Mn evaporation during the crystal growth. For example, three furnace cooled samples with the [001] orientation were tested and the stress-Ms temperature relations were shown in Figure 3-2. The red and green curve come from different single crystal batches, thus the extrapolated Ms temperatures are slightly different from each other. However, the slopes are similar. The blue and green curves represent the samples from the same crystal but from different layers. Although the slope of the curves is slightly different, Ms Temperatures in the stress free conditions are pretty close according to extrapolation of solid curves indicated by dashed lines.

The results in Figure 3-2 could be identified according to cooling rate or orientations. Furnace cooled samples occupy the left part of the figure, since the Ms temperatures ranges from 173K to 203K. The sample to sample variation in these samples with the same cooling rate arises most probably from compositional inhomogeneity between different single crystal batches and at different locations of a large single crystal where the samples are cut from. The samples from the same batch of single crystal have a small Ms range between 263K and 273K, as shown by the brown, blue and green curves, while the other furnace cooled sample from another single crystal batch shows an Ms of about 173K. Similarly, oil quenched samples have medium Ms temperatures ranging from 233K to 243K as shown at the center of figure. Water quenched samples have the highest Ms temperature around 273K. Obviously, Ms temperature varies with different cooling rates from the solutionizing temperature. Atomic ordering plays an important role in this observation of the stress influence of cooling rate. Ito *et al* [59] reported that $Ni_{45}Co_5Mn_{36.7}In_{13.3}$ alloy could exhibit either a B2 to $L1_0$ or $L2_1$ to 6M phase transformation depend on the annealing temperature. An 80K difference in Ms Temperature was discovered between these two cases in their work. This indicates that constitutive phases for NiMnCoIn may have different atomic ordering

due to heat treatment. In the current work, all the samples were homogenized at 900°C but quenched or cooled by different methods. It is entirely possible that different ordering exist in these samples which would be further examined through X-Ray diffraction in the following section.

In terms of crystallographic orientation, it is apparent that the [111] oriented samples demonstrate much steeper slopes than the [001] oriented samples. The slope of the [111] furnace cooled sample is 3.97 MPa/K comparing to an average of 2.02 MPa/K for the [001] samples and the slope of the water quenched [111] samples is 7.43 MPa/K while it is 3.22 MPa/K for the [001] samples after water quenching. From classical Claussius-Clapeyron equation, it is well known that

$$\frac{d\sigma_c}{dT} = \frac{\Delta S}{\varepsilon \cdot V_m} \qquad 3-1$$

where σ_c represents for the critical stress for the onset of phase transformation, T is temperature. ε donates the transformation strain and V_m is the molar volume of the alloy. ΔS is the change of entropy. Thus, the slope of fitting lines in Figure 3-2 indicates the value on the left-hand side of the equation. For samples with the same composition and heat treatment, ΔS should not vary notably much among them. Assuming that the parent phase and martensite phase is structurally compatible with each other reasonably and the change of molar volume is negligible, the ratio $\frac{\Delta S}{V_m}$ could be taken as a constant. Transformation strain is orientation dependent and could be calculated using the energy minimization theory [25]. The theoretical transformation strain of the oriented [001] $Ni_{45}Co_5Mn_{36.7}In_{13.3}$ single crystals was reported to be much higher than that of the [111] orientation [60]. As a result of that, the value of $\frac{d\sigma_c}{dT}$ for the [111] orientation sample should be higher than that of the [001] orientation, which matches with the experimental results.

Another observation from the figure is that, for the same heat treatment, Ms temperatures are almost the same for different orientations. This is because of the fact that the energy required for the transformation is mainly dependent on the structure and composition of the material.

Crystal Structure Characterization Using Synchrotron High-Energy X-Ray Diffraction---The Effect of Cooling Rate

In order to determine the structure of $Ni_{45}Mn_{36.5}Co_5In_{13.5}$ single crystals in austenite and martensite phase after solutionizing and different cooling rate, 2D diffraction patterns were collected using a synchrotron high-energy XRD technique. Figures 3-3a and 3-3c show the 2D pattern of austenite for a water quenched sample with [001] orientation at room temperature (300K). The peaks are indexed within the green rectangular regions shown in Figures 3-3a and 3-3c, and the corresponding intensity versus 2 Theta angle plots are shown in Figures 3-3b and 3-3d, respectively. The [111] and [113] peaks in Figure 3-3b are characteristic for $L2_1$ structure. However, at some locations on the sample, the [113] peak could not be observed, as shown in Figure 3-3d. Since the [111] peak is also an indication of B2 structure, the structure of austenite phase for the water quenched sample could be a mixture of $L2_1$ and B2. Moreover, the very broad [111] and [113] peaks in Figures 3-3b and 3-3d also indicate a disorder in the $L2_1$ (or B2) structure. Figure 3-4a exhibits the 2D diffraction pattern of martensite phase of the same water quenched sample at 100K. The rectangular region surrounded by yellow lines is magnified in Figure 3-4b and the intensity verses 2 Theta angle plot is shown in Figure 3-4c. The water quenched sample has a 6M modulated structure in martensite at 100K. Wang et al reported the 14M modulated martensite for the $Ni_{45}Co_5Mn_{36.6}In_{13.4}$ single crystal with the same quenching method [61]. However, the sample in that work was homogenized at 1173K. Karaca *et al* [60] also reported that for the water quenched $Ni_{45}Co_5Mn_{36.5}In_{13.5}$ single crystal, austenite is $L2_1$ structure and martensite is 6M. Ito et al observed that the different annealing temperature would result in different atomic ordering in austenite and martensite for NiMnCoIn alloys [59]. The different annealing temperature may be responsible for the new structure found in the current work.

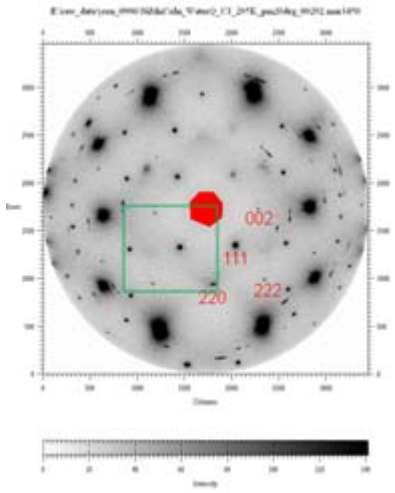

(a)

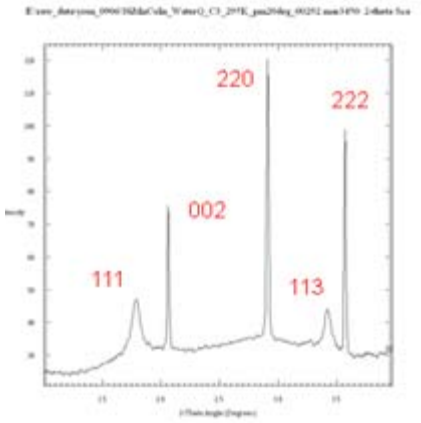

(b)

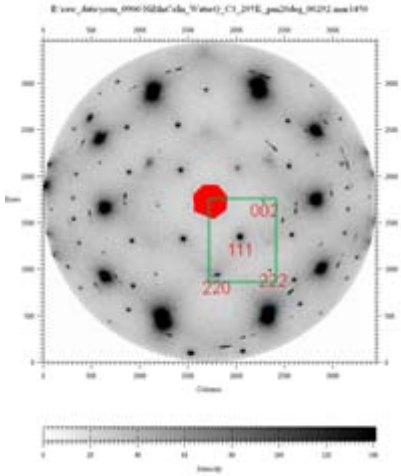

(c)

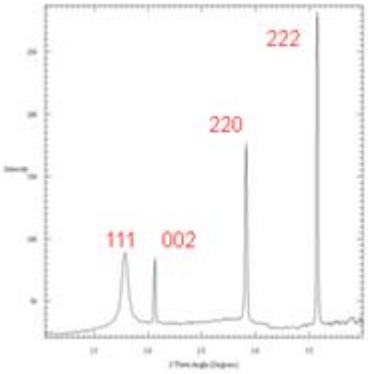

(d)

Figure 3-3 2D X-Ray diffraction for the austenite of [001] water quenched $Ni_{45}Co_5Mn_{36.5}In_{13.5}$ (a)(c), and the corresponding intensity versus 2 theta plot (b)(d). Results show that the austenite is a mixture of $B2/L2_1$

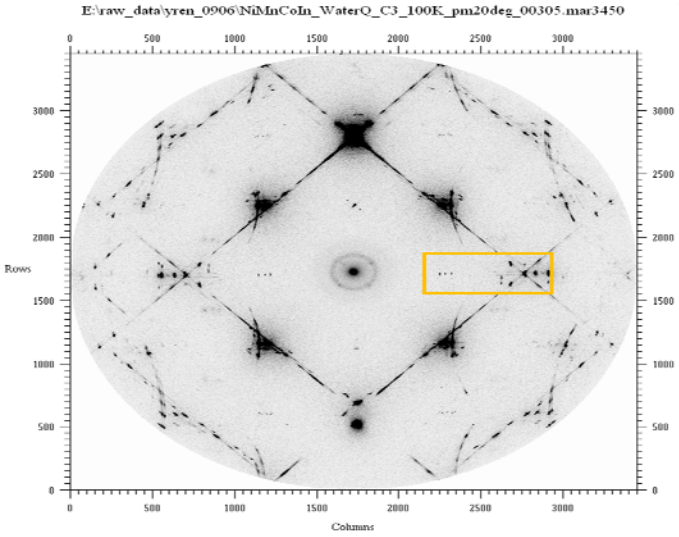

(a)

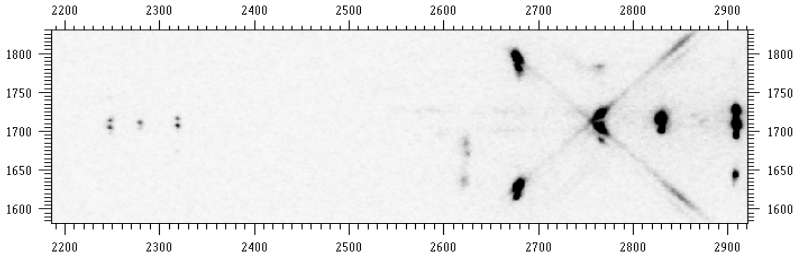

(b)

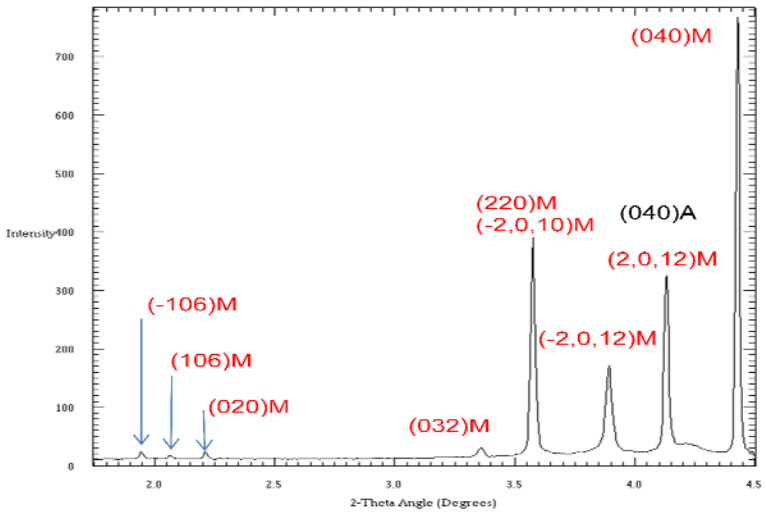

(c)

Figure 3-4 2D X-Ray diffraction for the martensite of [001] water quenched $Ni_{45}Co_5Mn_{36.5}In_{13.5}$ (a)(b), and the corresponding intensity versus 2 theta plot (c). The martensite shows a 6M structure

The same structural characterization work was performed on the oil quenched samples. Figure 3-5a shows the indexed 2D pattern of the sample at 300K. The intensity versus 2 Theta plot exhibits the structure of the rectangular region in Figure 3-5a, as shown in Figure 3-5b. Similar to the water quenched case, B2 and $L2_1$ austenite phases could be coexisting. However, the [111] peak is even broader than that in water quenched sample in Figure 3-3b. This indicates that the oil quenched sample here could be more disordered than the water quenched sample. Figure 3-6a shows the 2D pattern of the same oil quenched sample at 100K. A clear phase transformation could be observed from Figure 3-5a to Figure 3-6a. However, it is very complicated to identify the structure from the figure. It is more likely that multiple similar structures coexist in the martensite phase in the sample, as shown in Figure 3-6b. One possibility is that several different modulated martensite structures e.g. 5M, 6M, and 7M form the mixture structure in the martensite phase of the oil quenched sample.

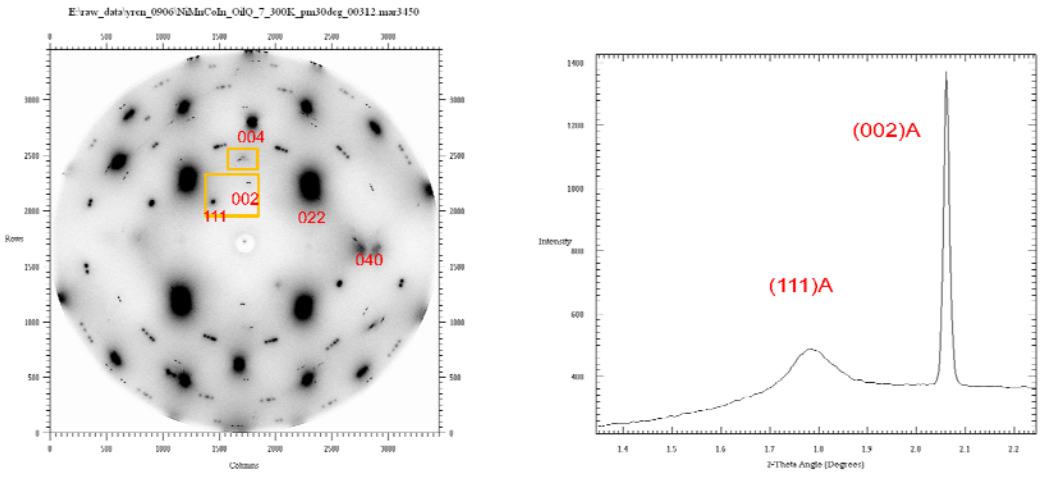

(a) (b)

Figure 3-5 2D X-Ray diffraction for the austenite of [001] oil quenched $Ni_{45}Co_5Mn_{36.5}In_{13.5}$ single crystal (a), and the corresponding intensity versus 2 theta plot (b). Results show that the austenite is a more disordered mixture structure of $B2/L2_1$

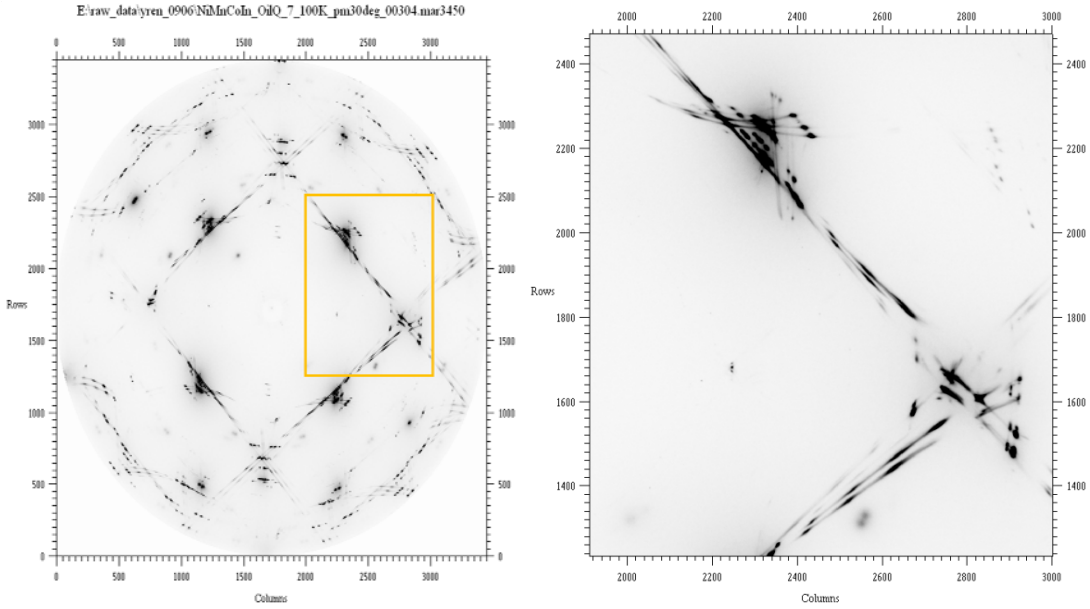

(a) (b)

Figure 3-6 2D X-Ray diffraction for the martensite of [001] oil quenched $Ni_{45}Co_5Mn_{36.5}In_{13.5}$ single crystal, 3-6b is the magnification of the rectangular region in figure 3-6a, which shows a mixed structure in martenite phase

Further tests were conducted on the furnace cooled sample. However, no transformation could be observed down to 100K. The reason for the stability of austenite upon cooling down to very low temperatures is not very clear even though an obvious transformation is observed under stress. This is believed to be related to the existence of isothermal martensitic transformation, but this is to be shown with further studies.

Magneto-Thermal Characterization of $Ni_{45}Mn_{36.5}Co_5In_{13.5}$ Single Crystals

In order to study the magnetic properties of the samples as a function of cooling rate, a Quantum Design Superconducting Interference Device (SQUID) was employed. The tests were conducted on $Ni_{45}Mn_{36.5}Co_5In_{13.5}$ samples after oil quenching, water quenching and furnace cooling. The results are shown in Figure 3-7 through 3-9.

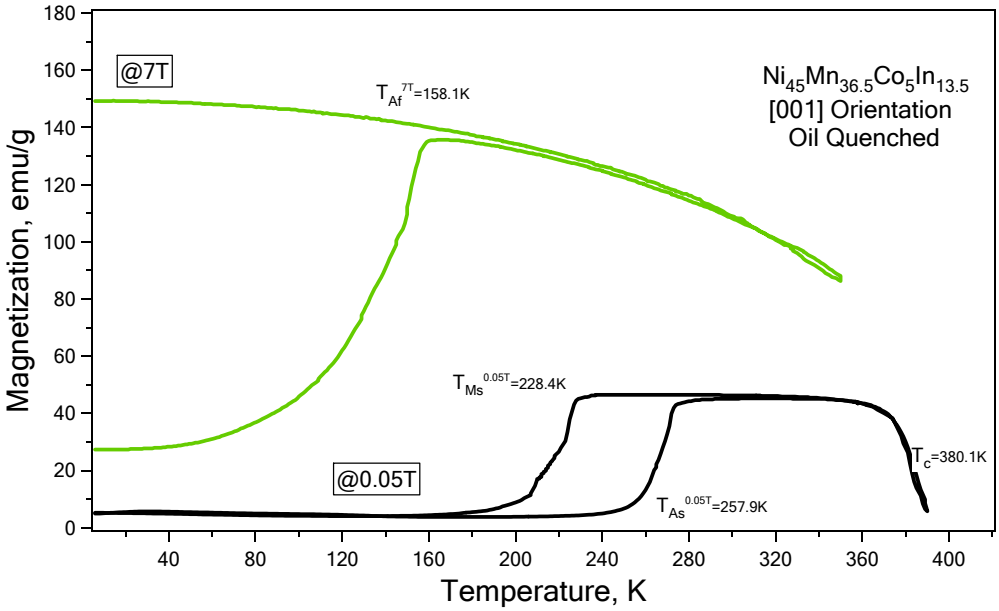

Figure 3-7a Thermomagnetization curves of oil quenched [001] oriented $Ni_{45}Mn_{36.5}Co_5In_{13.5}$ single crystals under 0.05T and 7T. Oil quenching was performed after 900°C solutionizing heat treatment

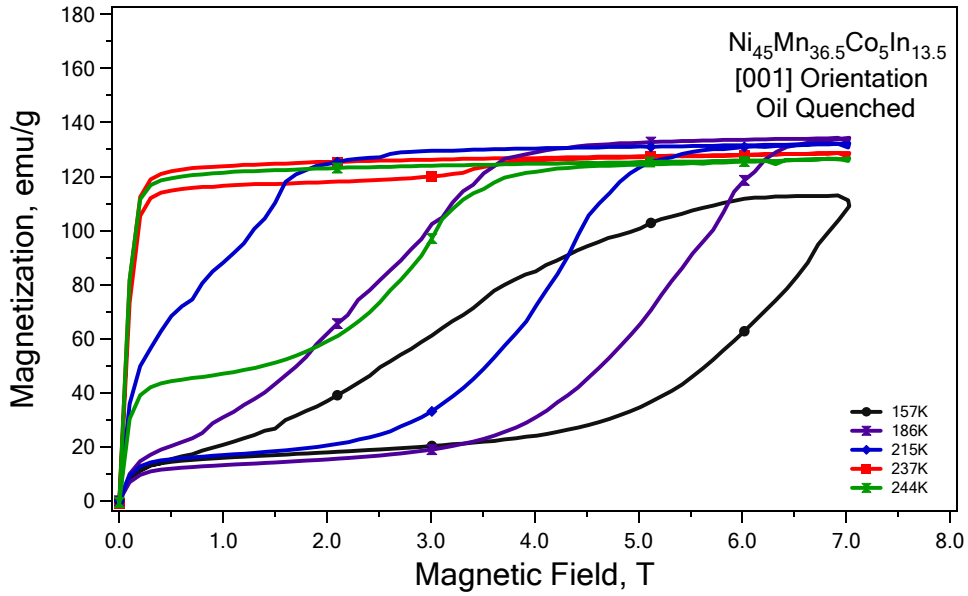

Figure 3-7b Magnetization curves of oil quenched [001] oriented $Ni_{45}Mn_{36.5}Co_5In_{13.5}$ single crystals in different temperatures near Ms temperature. Oil quenching was performed after 900°C solutionizing heat treatment for $Ni_{45}Mn_{36.5}Co_5In_{13.5}$ single crystal

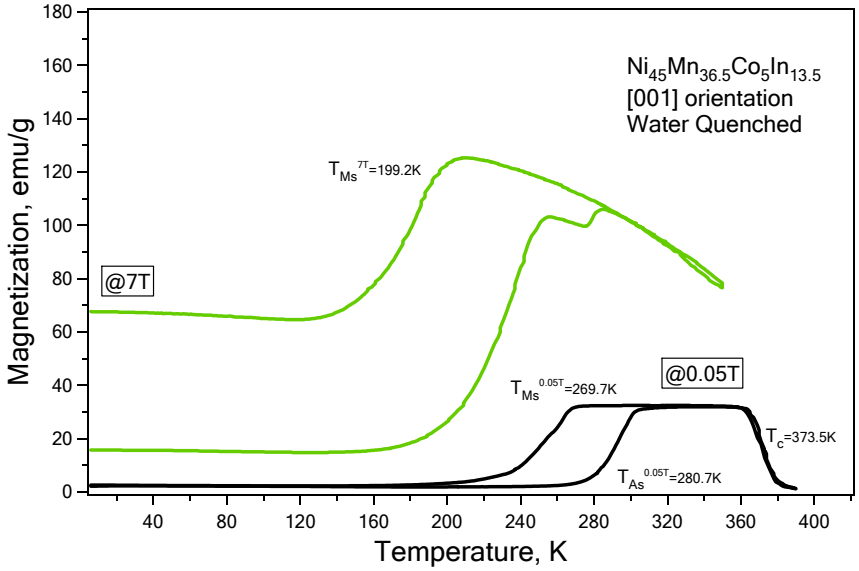

Figure 3-8a Thermomagnetization curves of wate quenched [001] oriented $Ni_{45}Mn_{36.5}Co_5In_{13.5}$ single crystals under 0.05T and 7T. Water quenching was performed after 900°C solutionizing heat treatment

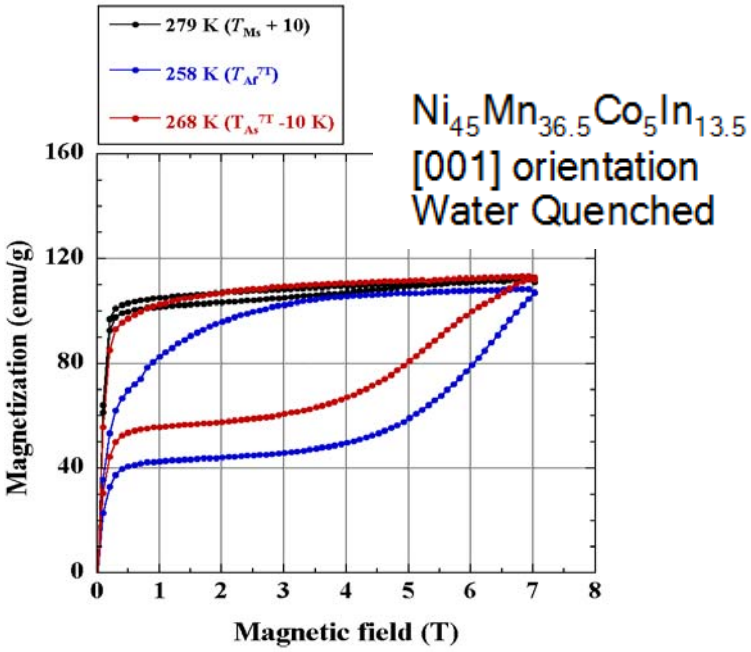

Figure 3-8b Magnetization curves of water quenched [001] oriented $Ni_{45}Mn_{36.5}Co_5In_{13.5}$ single crystals in different temperatures near Ms temperature. Water quenching was performed after 900°C solutionizing heat treatment for $Ni_{45}Mn_{36.5}Co_5In_{13.5}$ single crystal

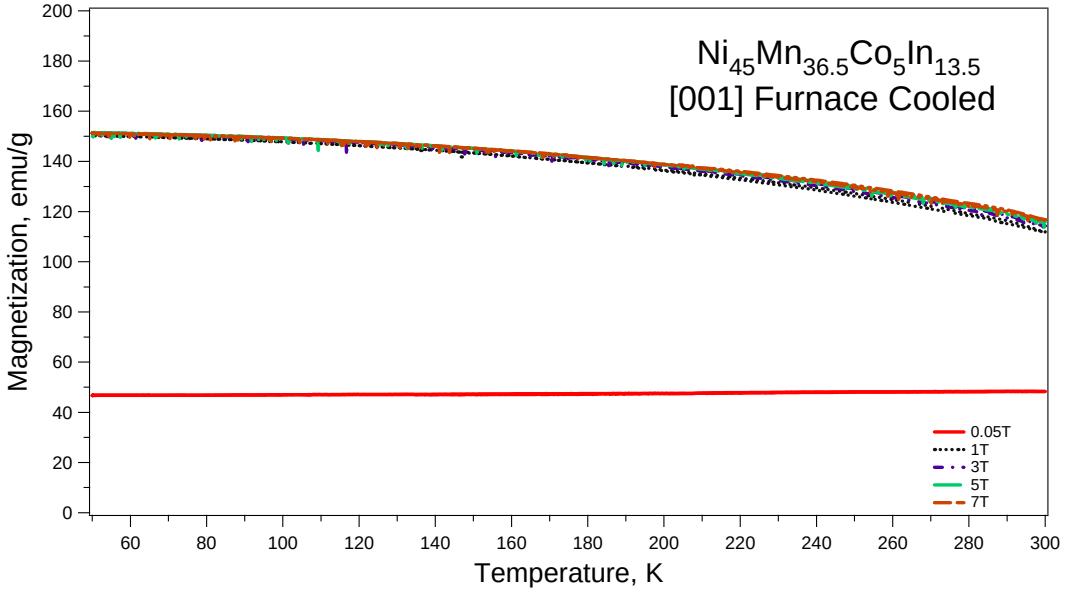

Figure 3-9 Thermomagnetization curve for $Ni_{45}Mn_{36.5}Co_5In_{13.5}$ furnace cooled single crystal after 900°C solutionized for 24 hours

Figure 3-7a shows the thermomagnetization curves of the oil quenched $Ni_{45}Mn_{36.5}Co_5In_{13.5}$ single crystal oriented along the [001] direction. Two tests were conducted under 0.05 Tesla and 7 Tesla, respectively. The black curve exhibits the magnetic behavior of the material under 0.05 Tesla. Two important phase transformations occur when the sample is cooled down. Initially, the sample is in non-ferromagnetic state at high temperatures around 400K. This non-ferromagnetic phase could be paramagnetic [38]. When cooled down, a phase transformation takes place at around 380K as indicated by the sharp increase in magnetization. The material transforms from non-ferromagnetic phase to a ferromagnetic phase. The critical temperature here, determined by the largest changing slope on the curve, is known as Curie temperature. For magnetic materials, Curie temperature is usually the critical temperature above which the materials will lose their ferromagnetic ability.

The other transformation takes place when the sample is further cooled down to about 228 K, as indicated by the drastic drop in magnetization. This is the martensite

transformation. The material transforms from ferromagnetic austenite to non-ferromagnetic martensite (either paramagnetic or antiferromagnetic). Recall that in Figure 3-2, the Ms temperature under zero stress is expected to be in the range of 243K to 233K for oil quenched samples. The Ms temperature determined from the SQUID results is around 228K, which is close to the thermo-mechanical characterization results and thus verifies that such transformation is indeed a martensite transformation. When an external magnetic field is applied, it aligns the direction of magnetic moments in a magnetic domain along the magnetic field direction. It is much easier to align the directions in a ferromagnetic phase than a non-ferromagnetic phase. In other words, external magnetic field favors the formation of ferromagnetic austenite phase so that the martensite transformation is suppressed by magnetic field. As a result, more energy is required from undercooling and the Ms temperature decreases.

Thermognetization experiments was also conducted under 7 Tesla and the result is shown by the green curve in Figure 3-7a. The sample was first cooled down to 10K and loaded to 7 T. Magnetization of martensite increases notably as compared to that of 0.05 T at the same temperature due to the alignments of magnetic moments with the field. When heated up, the sample shows a reverse martensitic transformation from martensite back to austenite and the transformation finishes at 158K. Magnetization level decreases slowly with the increasing temperature after the reverse martensitic transformation is completed because of getting close to the Curie temperature. Higher temperature increases the internal energy of the sample, which will disturbs the alignment of magnetic moments and leads to the decrease in net magnetization.

It is worth noting that cooling curve for the oil quenched sample looks completely different under 0.05 T and 7 T. For the previous case, though a hysteresis loop exists, the magnetization returns to the same level as the original point at 10K. On the other hand, when the sample was cooled down under 7 T to low temperature (10K), no martensitic transformation is observed and the magnetization remained at a high level of around 150 emu/g. This is so called the kinetic arrest of austenite [62]. According to thermodynamics, in order for the martensitic transformation to occur, the energy from

undercooling, which is the change of chemical energy upon phase transformation, must be larger than the sum of the energy from external magnetic field, i.e Zeeman Energy, stored elastic energy and other dissipated energy due to defect generation and lattice friction. In other words, if Zeeman energy is too large, the chemical energy difference upon undercooling cannot compensate for the total energy required, thus martensitic transformation does not take place upon cooling. This could be the reason for kinetic arrest of austenite.

The same thermomagnetization experiments were also conducted on water quenched sample and the results are shown in Figure 3-8a. Ms and Af temperatures are approximately determined to be 269 K and 280 K under 0.05 T. Under 7 T, Ms and Af are about 199 K and 256 K, respectively. Ms and Af are suppressed by 72 K and 24 K due to magnetic field, respectively. Ms decreases much more than Af, which indicates that the temperature hysteresis under 7 T is larger than that of 0.05 T. The reason behind that is not clear yet. One possibility is that, since magnetic field favors the formation of austenite, the magnetic domain wall movement becomes difficult and causes more dissipation energy during transformation.

Compared to the oil quenched sample, two differences are worth discussing. First, under low magnetic field, water quenched sample has a higher transformation temperature. The Ms, Mf, As, and Af temperatures are all higher in the water quenched sample than those in the oil quenched sample. These results match the trends in the transformation temperatures in Figure 3-2. Second, the complete kinetic arrest of austenite does not occur throughout the sample. In Figure 3-8a, it is obvious that the magnetization starts to decrease drastically at about 199 K due to the martensitic transformation. However, the magnetization value is not as low as the magnetization level of fully martensitic sample stabilizing at a higher value about 70 emu/g. Both differences are probably due to the ordering effect through different cooling rate.

It is also worth noting that SQUID results do not show any martensitic transformation for the furnace cooled samples. Figure 3-9 is the thermomagnetization curve for the [001] oriented furnace cooled $Ni_{45}Mn_{36.5}Co_5In_{13.5}$ single crystal.

Magnetization of the sample remains unchanged down to 50K under 0.05 T and 0.2 T. This means that the material is stable in ferromagnetic phase regardless of temperature. The result matches with the observations in X-ray diffraction studies where there was no phase transformation down to 50K in the same sample. However, it is difficult to rationalize the lack of phase transformation because martensitic transformation was observied in the thermo-mechanical experiments under stress.

Isothermal magnetization tests were also conducted for specimens with different cooling rate in the vicinity of martensitic transformation temperatures. As shown in Figures 3-7b and 3-8b, metamagnetic transformation could be verified in both the oil quenched and water quenched samples.

Effect of Magnetic Field on the Superelastic Response

As mentioned in the previous sections, the pseudoelastic responses of the present crystals are expected to shift up when a constant magnetic field is applied. Magnetostress is taken as the measurement of this shift which also indicates the extra stress required for martensitic transformation and it is directly related to the extra energy needed. However, the effect of magnetic field on magnetostress is complicated and can be influenced by many factors. Here, three factors will be discussed: temperature, orientation and heat treatment (cooling rate).

In order to determine how temperature affects the pseudoelastic behavior under magnetic field, the experiments was conducted on a furnace cooled [001] oriented $Ni_{45}Mn_{36.5}Co_5In_{13.5}$ single crystal sample in a temperature range from 228K to 293K. The results are shown in Figure 3-10.

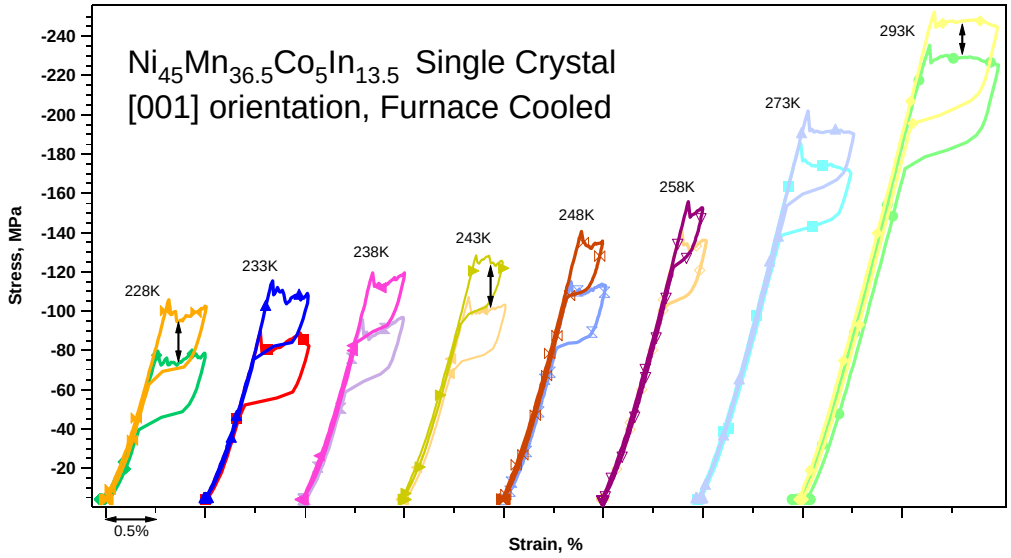

Figure 3-10 Pseudoelastic response of the [001] oriented $Ni_{45}Mn_{36.5}Co_5In_{13.5}$ single crystals with and without 1.6 T magnetic field at temperatures ranging from 228K to 293K on furnace cooled samples

Pseudoelastic tests were conducted with and without magnetic field (1.6 T). As is expected, at each temperature the curves under magnetic field shifted up. The maximum strain level was 1% in the tests from 228K to 258K while 1.5% at 273K and 2% at 293K. Before analyzing, it is worth noting that the value of magnetostress is irrelevant to strain levels in the tests, because the difference of critical stress for martensitic transformation with and without magnetic field does not depend on how much strain the sample goes to. In the current study, magnetostress is taken as the difference in stress with and without magnetic field at half of the maximum strain. Magnetostress is shown in Figure 3-11 as a function of temperature. It fluctuates around ±3 MPa up to 248K and then starts to decrease with temperature. The value of magnetostress reaches the minimum of 15 MPa at 293K. It is expected to decrease further with increasing test temperature. Since magnetostress is directly related to magnetic energy converted during phase transformation, the trend exhibited in Figure 3-11 should be related to the change in Zeeman energy difference between austenite and martensite at various temperatures. Such Zeeman energy difference could be determined from saturation magnetization

versus magnetic field. Unfortunately, neither XRD nor SQUID shows martensitic transformation in the furnace cooled sample to allow the measurement of the saturation magnetization of martensite. However, the saturation magnetization of austenite and martensite could be measured for the oil quenched samples using SQUID as shown in the previous section, and it's temperature dependence is shown as the black curve in Figure 3-11. In this case, the saturation magnetization difference between austenite and martensite changes slightly at low temperature and gradually decreases with the increasing temperature. As a result, the Zeeman energy difference between martensite and austenite decreases with increasing temperature, so does the magnetostress. However, although magnetostress decreases with the increasing temperature, the change is very small (only 5 MPa in 65°C).

To reveal the effect of crystallographic orientation on magnetostress, another set of pseudoelastic tests was run on the [111] oriented $Ni_{45}Mn_{36.5}Co_5In_{13.5}$ furnace cooled single crystal at 248K (Ms+60K). Figure 3-12 shows the results. The magnetostress under 1.6 T is about 52 MPa in this case. Compared to 22 MPa for the [001] oriented sample at the same temperature, the [111] oriented sample demonstrate twice as high magnetostress. This indicates that orientation has a strong effect on magnetostress. To have a better understanding, some theoretical calculations will be introduced in the following sections. Briefly, the total magnetic energy could be determined by multiplying magnetostress and strain. For the same composition and same heat treatment, the total Zeeman energy should remain the same at the same temperature regardless of orientation. However, orientation changes the value of transformation strain. In other words, smaller maximum strain value will leads to a larger magnetostress. In this case, [111] orientation has a much lower transformation strain according to the energy minimization theory [60], which leads to a big increase in magnetostress.

To see the heat treatment effect on magnetostress, the same pseudoelastic tests under magnetic field were also conducted on [001] oriented oil quenched sample at 318K (Ms+70K) and water quenched sample at 273K (Ms+60K). Results are shown in Figure 3-13 and Figure 3-14. Magnetostress at 1.6T for the oil quenched sample is

determined to be 26.3 MPa and for the water quenched sample, the number is 26.97 MPa up to 1.6T. Compared to the 18 MPa at 273K for furnace cooled, these values are much higher. Recall that temperature could affect the magnetostress, the magnetostress of oil quenched sample at 273K might be larger than the value at 318K, considering the results from SQUID as mentioned in above. However, since the saturation magnetization difference does not change much from 273K to 318K according to the thermomagnetization results from SQUID, the magnetostress is not expected to change much. Magnetostress is higher in water quenched and oil quenched samples than in furnace cooled samples. The reason behind is not clear, unfortunately. The low cooling rate in furnace cooling might account for it.

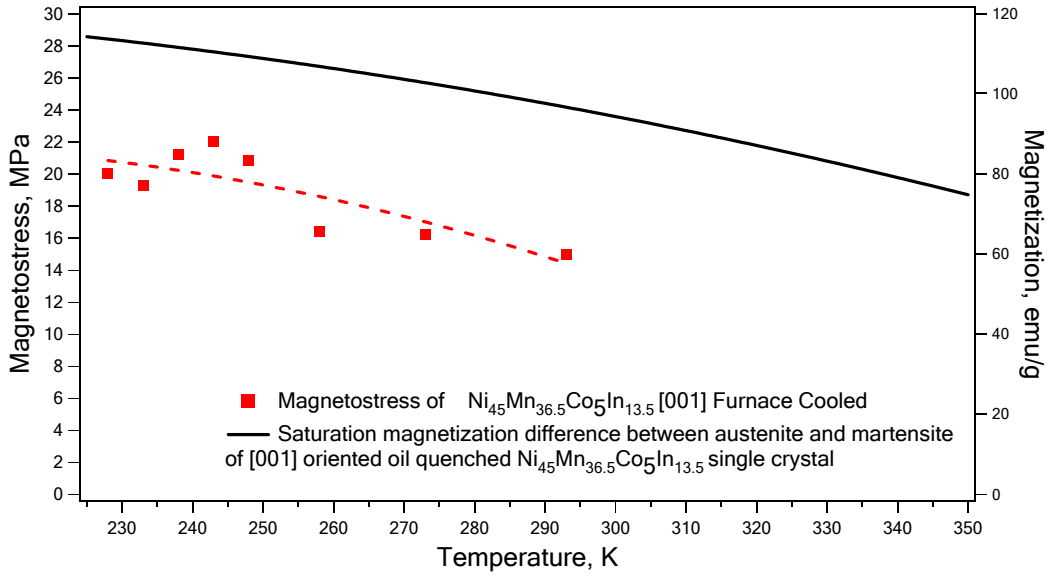

Figure 3-11 Magnetostress changes with temperature in $Ni_{45}Mn_{36.5}Co_5In_{13.5}$ [001] oriented furnace cooled single crystal shown by red squares and fit to the dashed curve. The black curve shows the difference of saturation magnetization between austenite and martensite for [001] oriented oil quenched $Ni_{45}Mn_{36.5}Co_5In_{13.5}$ single crystal

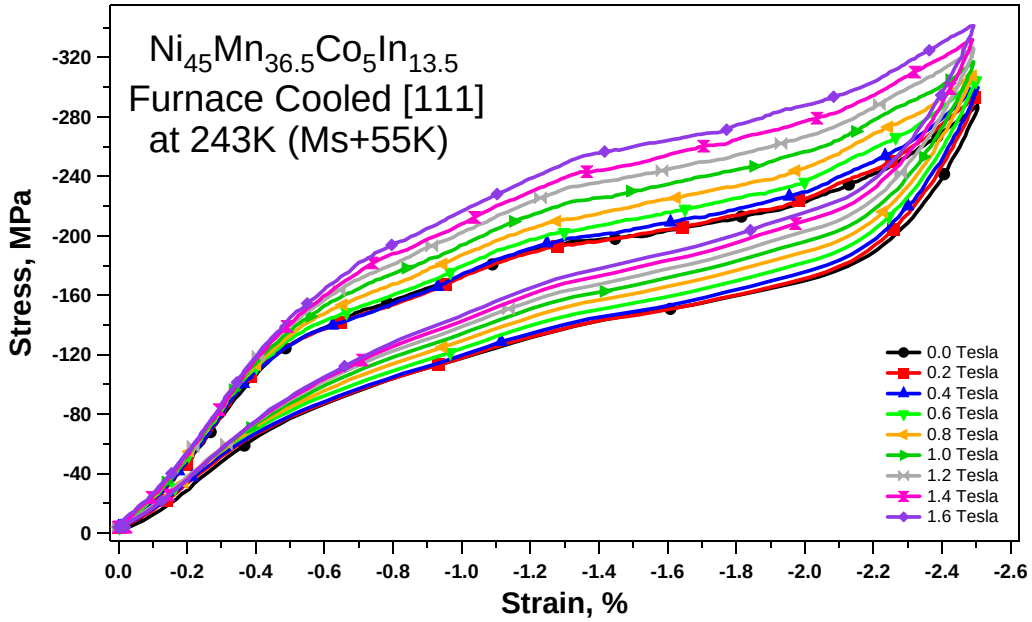

Figure 3-12 Pseudoelastic response of $Ni_{45}Mn_{36.5}Co_5In_{13.5}$ with [111] orientation furnace cooled sample under magnetic field from 0T to 1.6T

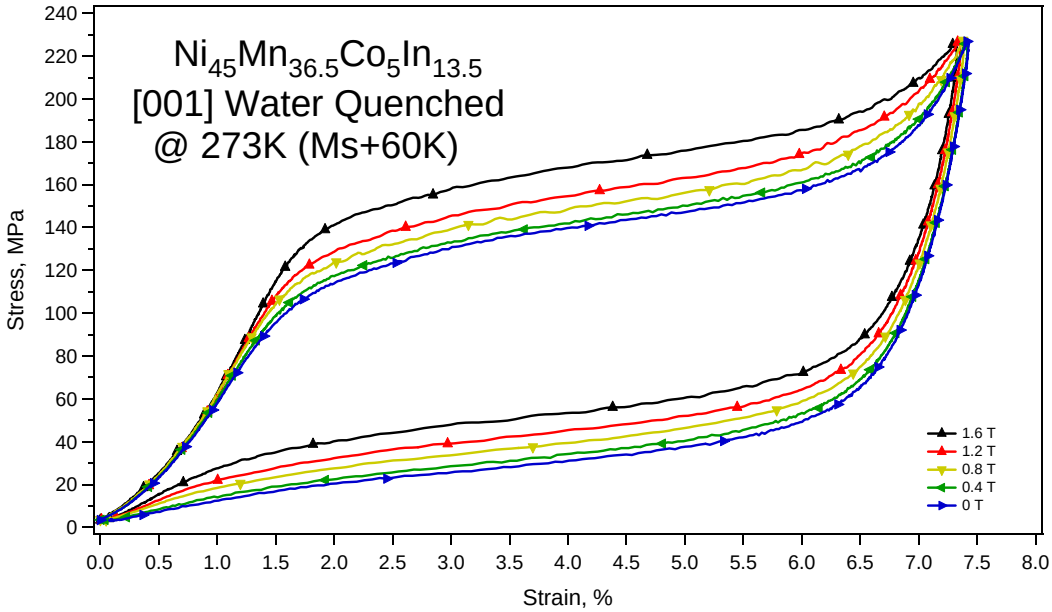

Figure 3-13 Pseudoelastic response of $Ni_{45}Mn_{36.5}Co_5In_{13.5}$ with [001] orientation water quenched sample under magnetic field from 0T to 1.6T

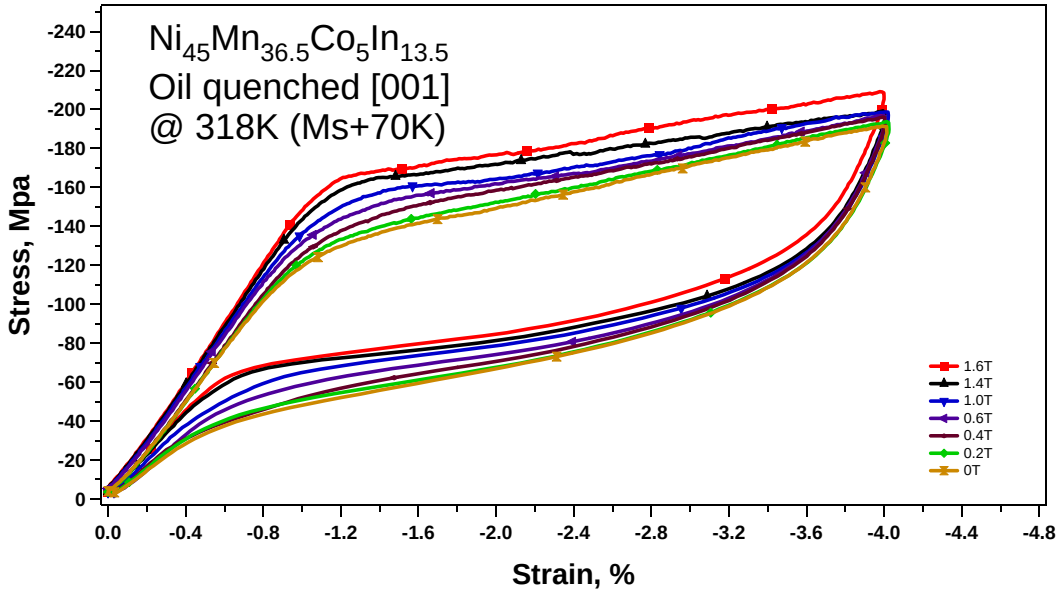

Figure 3-14 Pseudoelastic response of $Ni_{45}Mn_{36.5}Co_5In_{13.5}$ with [001] orientation oil quenched sample under magnetic field from 0T to 1.6

Here, we discuss the relation between magnetostress and magnetic field. Figures 3-12 through 3-14 exhibit the pseudoelastic response of $Ni_{45}Mn_{36.5}Co_5In_{13.5}$ single crystals with different orientations and heat treatments under magnetic field in the range from 0 T to 1.6 T. Magnetostress levels were determined for each test as a function of magnetic field and is ploted in Figure 3-15.

In all cases, magnetostress first changes nonlinearly with magnetic field up to about 0.4 T and then increases almost linearly with the magnetic field. This trend follows the same trend in the difference in the Zeeman Energies of austenite and martensite phases. Figure 1-17 schematically shows the M-H curves of austenite and martensite phases. The area between the two curves indicates the Zeeman Energy difference between martensite and austenite. Initally, magnetization changes linearly with magnetic field in the M-H curve. Since the lines for austenite and martensite phase have different slopes, the area in between increases nonlinearly with increasing magnetic field. This explains the non-linear relation between magnetostress and magnetic field at low magnetic field up to the saturation field. After reaching the saturation magnetic field, the

magnetization of austenite and martensite phases remain as a constant under increasing field. In this case, the area between the curves increases linearly with increasing magnetic field so that the magnetostress is also increases linearly with magnetic field.

In Figure 3-15, the linear part of the magnetostress values for each sample was fit by the best fit line. The slope of these varies from each other depending on orientation, heat treatment and temperature. From the figure, it could be concluded that furnace cooled specimens have the lowest slope around 12.26 MPa/T in the [001] oriented materials. Furthermore, the [111] specimen has a much larger slope than the [001] specimens. It was predicted by Karaca et al that the rate of increasing in magnetostress as a function of magnetic field for the [111] $Ni_{45}Mn_{36.5}Co_5In_{13.5}$ single crystals could reach 143.4 MPa/T [60]. However, the slope for the [111] specimen in the present work is only about 44.7 MPa/T. The reason for this large discrepancy is the heat treatment differences. Different atomic ordering can be achieved with water quenching, oil quenching or furnace cooling. And the atomic ordering affects the magnetostress by influencing the magnetic properties of the transformation phase. Moreover, the calculations and experiments that Karaca *et al* performed are based on the materials parameters for the water quenched $Ni_{45}Mn_{36.5}Co_5In_{13.5}$ single crystals oriented in [001] direction. In Figure 3-15, the water quenched and oil quenched samples both exhibit much higher slope than the furnace cooled sample in the [001] orientation. Although no experiment has been conducted so far for the [111] orientation samples other than the furnace cooled case, it could be predicted that for the water quenched and oil quenched [111] samples, it should be possible to reach a much higher slope, which might be closer to the predicted value.

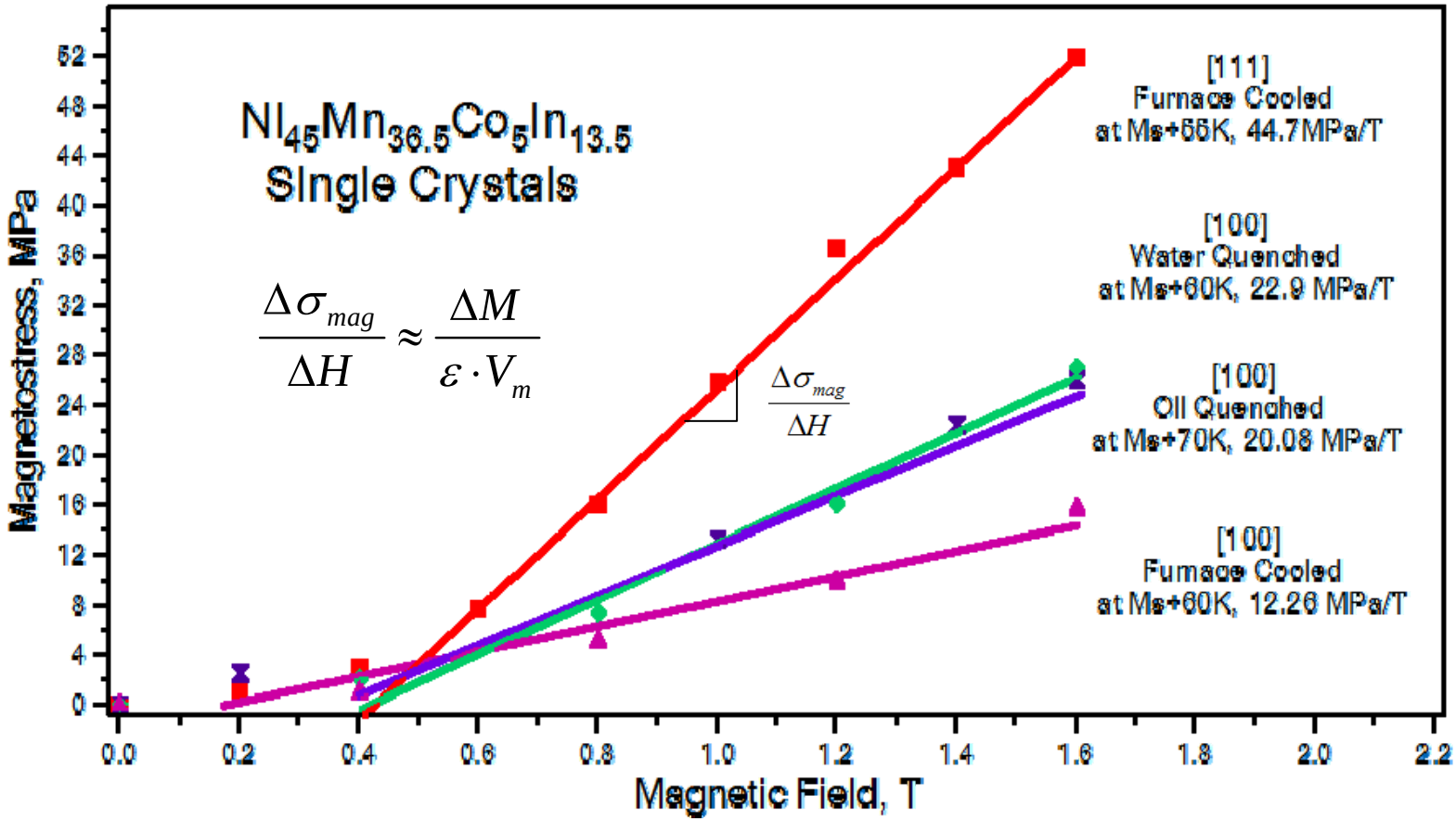

Figure 3-15 Magnetostress versus magnetic field response of the $Ni_{45}Mn_{36.5}Co_5In_{13.5}$ single crystals with two different compression axis and heat treatments. The magnetostress levels were extracted from the results shown in Figure 3-11 through Figure 3-14

Prediction of Magnetostress as a Function of Orientation and Heat Treatment

It was mentioned above that combined magnetostress and transformation strain is a measure of magnetic energy converted into mechanical work. In this section, how available magnetic energy changes with the heat treatment will be discussed and orientation and heat treatment dependence of magnetostress will be predicted. The purpose of doing this is to find out an easy way to predict the magnetostress without doing complicated magneto-thermo-mechanical experiments.

The magnetic energy could be expressed using either magnetostress or the saturation magnetization difference between austenite and martensite

$$\sigma_{MAG} \cdot \varepsilon_{tr} = \Delta M \cdot \Delta H \qquad 3\text{-}2$$

where σ_{MAG} is the magnetostress, ε_{tr} is the phase transformation strain and it is measured from pseudoelastic experiments. ΔM represents the difference of saturation magnetization between austenite and martensite phases. ΔH denotes the change in magnetic field. This equation describes the coupling between mechanical energy and magnetic energy in a simple fashion. When the material is deformed under magnetic field, magnetic energy acts as an extra barrier for martensitic transformation. Reorganizing the equation 3-2, we obtain,

$$\frac{\sigma_{MAG}}{\Delta H} = \frac{\Delta M}{\varepsilon_{tr}} \qquad 3\text{-}3$$

The left term represents the slopes in Figure 3-15. In the expression, on the right-hand side, ΔM could be determined directly from the SQUID results and ε_{tr} could be measured from the pseudoelastic experiments. Using these results, it is possible to predict $\frac{\sigma_{MAG}}{\Delta H}$. Taking the oil quenched sample as an example, the difference between the saturation magnetizations of both phases could be measured from the SQUID results as shown figure 3-16. The black line represents the saturation magnetization of austenite as a function of temperature from SQUID. The saturation magnetization of martensite is determined from the thermomagnetization results at low temperatures less than 215K and a best fit line is constructed between these points as shown in the figure. In order to predict the saturation magnetizations at higher temperatures, the best fit line is extrapolated to a higher temperature. Transformation strains are determined from the

stress-strain curves as shown in Figure 3-17. A horizontal line is drawn at the critical stress level for the onset of transformation and extended until the unloading curve is cut. The length of the line inside the loop is defined as the transformation strain.

It should be noted here that the magnetization value has a unit of emu/g in the SQUID experiments. To be consistent in terms of units on the both sides of equation (1), the unit of magnetization has to be converted to emu/cm^3. In order to achieve this, magnetization is modified by multiplying the density of the alloy. The density of $Ni_{45}Mn_{36.5}Co_5In_{13.5}$ is taken as 8.07 g/cm^3 as a rough estimate.

Assuming that magnetization difference in equation 3-3 is the distance between the black line and the dashed line in Figure 3-16 and transformation strain is 4.32 % from the experiments, $\frac{\sigma_{MAG}}{\Delta H}$ can be determined as 15.85 MPa/T. Alternatively, assuming that the saturation magnetization of martensite is negligible at high temperatures, $\frac{\sigma_{MAG}}{\Delta H}$ can be calculated as 19.12 MPa/T. Similar calculations have also been done on the other samples and the results are summarized in Table 3-1.

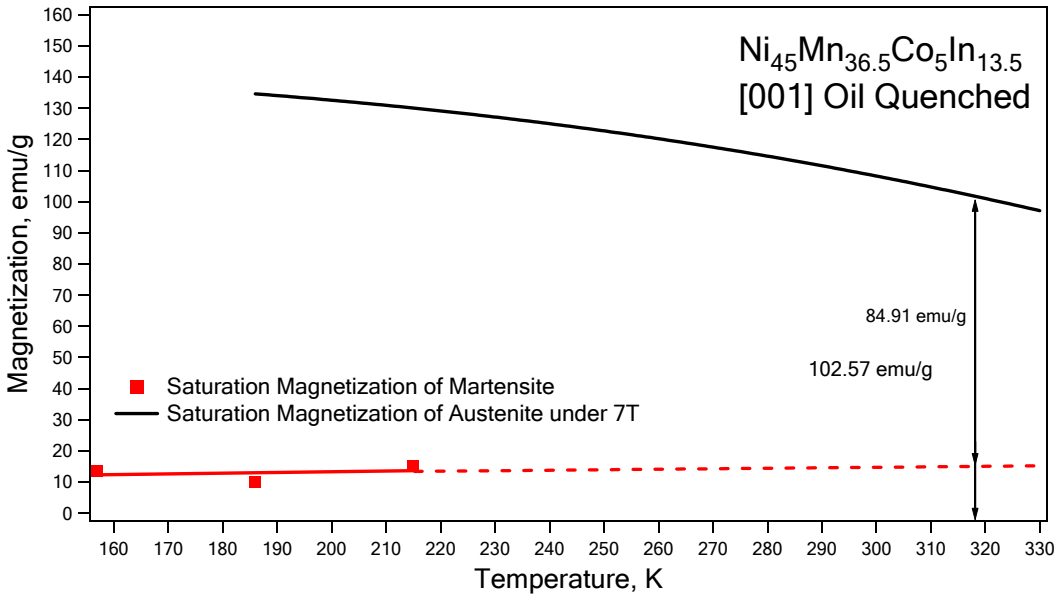

Figure 3-16 Saturation magnetizations of austenite and martensite phases as a function of temperature for the oil quenched [001] oriented $Ni_{45}Mn_{36.5}Co_5In_{13.5}$ single crystal

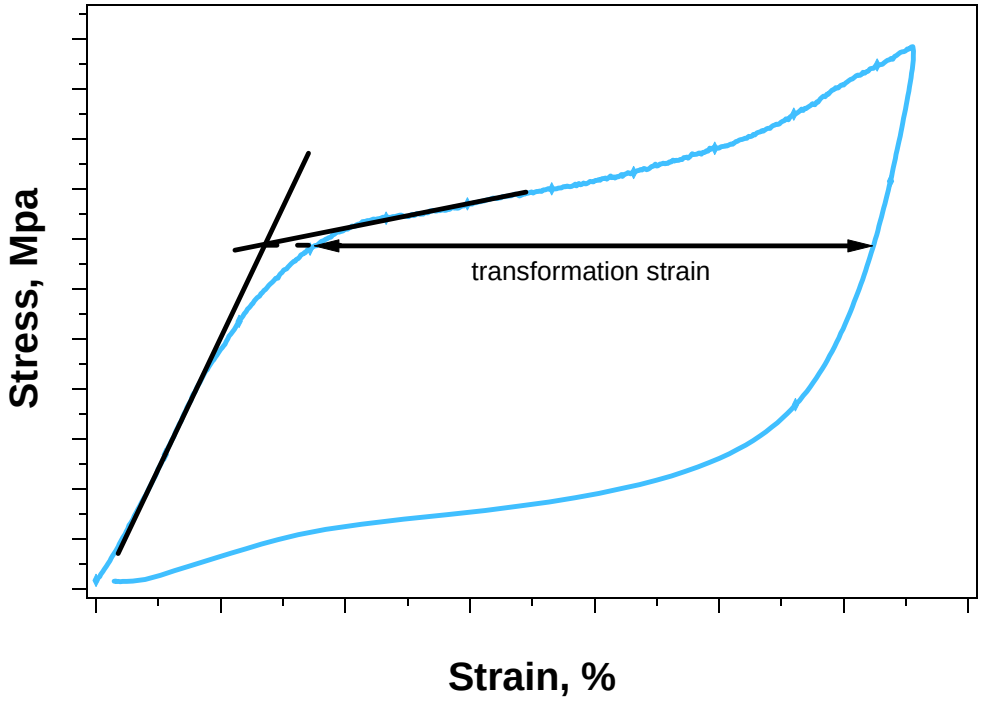

Figure 3-17 Stress-strain curve exhibiting the way to determine transformation strain

Table 3-1 Calculation results on $Ni_{45}Mn_{36.5}Co_5In_{13.5}$ single crystal with different orientation and heat treatments

	[100] Oil Quenched	[100] Water Quenched	[100] Furnace Cooled	[111] Furnace Cooled
ε_{tr}	4.32%	4.79%	4.83%	1.58%
$\frac{\sigma_{MAG}}{\Delta H}_{calculation1}$	15.85 MPa/T	16.26 MPa/T	9.04 MPa/T	27.77 MPa/T
$\frac{\sigma_{MAG}}{\Delta H}_{calculation2}$	19.12 MPa/T	18.64 MPa/T	18.96 MPa/T	58.17 MPa/T
$\frac{\sigma_{MAG}}{\Delta H}_{experimental}$	20.08 MPa/T	22.90 MPa/T	12.26 MPa/T	44.70 MPa/T

The method 1 for the prediction of $\frac{\sigma_{MAG}}{\Delta H}$ in Table 3-1 considers the extrapolated value as the saturation magnetization of martensite, while method 2 neglects the saturation magnetization of martensite at high temperatures. The reason for using two methods for calculation lies mainly in the uncertainty of martensite's saturation magnetization. The saturation magnetization of martensite may not change linearly with temperature, as indicated by the dashed line in Figure 3-16. The purpose of such classification is to set an approximate boundary for the value of $\frac{\sigma_{MAG}}{\Delta H}$. It could be seen from Table 3-1 that the calculated results matches well with experimental results in oil quench and furnace cooled case. The experimental value of $\frac{\sigma_{MAG}}{\Delta H}$ is a little higher than the calculated results. The reason for that is probably because the magneto-thermo-mechanical results and SQUID results come from different water quenched samples. Although they are with same orientation and heat treatment, magnetic properties may vary from sample to sample.

Stress-assisted Reversible Magnetic Field Induced Phase Transformation in $Ni_{45}Mn_{36.5}Co_5In_{13.5}$ Metamagnetic Shape Memory Alloys

As mentioned in the previous chapters, a reversible metamagnetic shape memory effect is valuable for practical applications in actuators. Assisted by external stress, it is possible to achieve reversible magnetic field induced phase transformation [32]. The necessary and sufficient condition for reversible FIPT is that the magnetostress is larger than the pseudoelastic stress hysteresis. In other words, available magnetic energy must be higher than the energy dissipated during reversible phase transformation. It is well established that magnetic field favors the formation of austenite in NiMnCoIn alloys, which means it is entirely possible for the magnetostress to be larger than stress hysteresis as long as the magnetic field applied is strong enough. Unfortunately, such requirement of strong magnetic field will seriously impede the practical applications of the alloy. However, no report has been focused on the reversible FIPT for NiMnCoIn alloys under low magnetic fields. According to previous discussions, magnetostress is

dependent on orientation, temperature and heat treatment. In the present study, the temperature is taken as a experimental variable. An attempt is made to explore the possibility of stress-assisted reversible FIPT in NiMnCoIn alloys under low field here. The [001] oriented furnace cooled sample was selected and pseudoelastic tests were performed at 223K, 233K and 248K under 0T and 1.6T, respectively. The results are shown in Figure 3-18. The reason of choosing the [001] orientation instead of the [111] oriented sample is the larger maximum strain levels. Moreover, the furnace cooled sample shows smaller stress hysteresis than oil quenched and water quenched samples indicated in Figures 3-12 through 3-14. Furthermore, brittleness is a major issue with NiMnCoIn alloys. The thermal stress due to water or oil quenching sometimes causes microcracks in the sample making it difficult to conduct reliable experiments. Furnace cooled samples have significantly higher toughness than water and oil quenched samples.

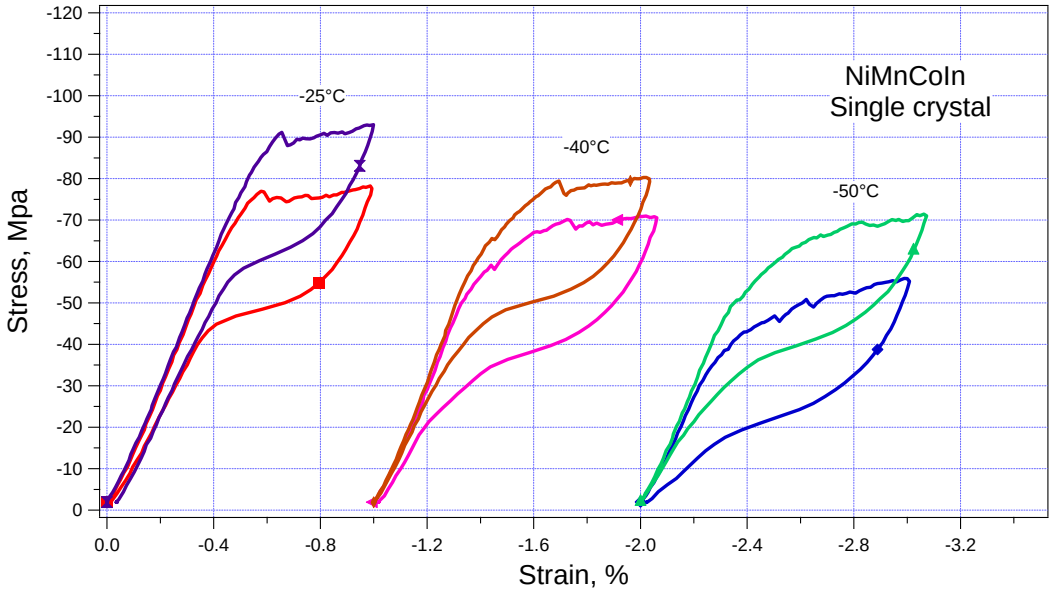

Figure 3-18 Pseudoelastic response of the [001] oriented samples of $Ni_{45}Mn_{36.5}Co_5In_{13.5}$ single crystals with and without 1.6T magnetic field at different temperatures

The critical stress level for the onset of martensitic transformation without magnetic field decreases with temperature, as expected from Clausius-Clapeyron relation. Stress hysteresis also slightly decreases with temperature. However, magnetostress increases with decreasing temperature from 223K to 248K. This could be explained using the thermomagnetization test results from SQUID. The difference between the saturation magnetizations the transforming phase increases with decreasing temperature, which indicates higher available magnetic energy at low temperatures. Down to 223K, pseudoelastic loops with and without magnetic field does not separate. This means, magnetic energy is still not enough to compensate for the dissipated energy under 1.6 T magnetic field. The reversible FIPT did not happen at this temperature under 1.6T. No further experiments are performed at lower temperatures because the temperature is approaching to A_f temperature. The pseudoelastic loops will not close during unloading if the operating temperature is lower than A_f and irrecoverable strain remains after unloading. Although stress-assisted reversible FIPT does not take place, it could be seen from the data that only about 10 MPa difference exists between magnetostress and stress hysteresis. According to the previous results, the magnetostress of [111] furnace cooled sample is about 36 MPa higher than the [001] sample at the same conditions. So [111] furnace cooled sample may show separated loops at similar temperatures. However, further tests are required to verify this prediction.

CHAPTER IV
EFFECT OF THERMO-MECHANICAL LOADING CONDITIONS ON THE TRANSFORMATION STRAIN AND HYSTERESIS IN $Co_{48}Ni_{33}Al_{29}$ SHAPE MEMORY ALLOYS

Design and Assembly of a Thermo-Mechanical Testing Setup Based on MTS Insight™ Electromechanical Test Frame

To characterize the effect of loading conditions on thermo-mechanical behavior of CoNiAl ferromagnetic SMAs, another MTS test frame based compression system was designed. The reason of using a new setup instead of the previous one is that the strain measurements by capacitive sensor is not as accurate as those using an extensometer directly attached to the samples, especially for determining elastic modulus of the material through pseudoelastic experiments. The core of the test system is a MTS Insight™ Electromechanical test frame. The load cell can measure up to 30kN force. A extensometer is attached on the 4x4x8 compression samples to measure strain during tests. The sample placed in between the grips is cooled by heat conduction. Testing temperature is controlled by an Omega 8200CN serious controller for each grip. Cooling is achieved by blowing liquid nitrogen though the copper coils wrapped around the grips. Two solenoid valves commanded by temperature controllers are used to control the blowing rate of liquid nitrogen. Heating bands wrapped outside the copper coils function as the heating elements and are also commanded by the temperature controllers. The sample temperature is detected by a K type thermocouple. A T-shape aluminum frame is designed to hold the thermocouple, as shown in Figure 4-1. A rubber band is used to force the thermocouple to the surface of the sample. To improve heating and cooling efficiency, a glass wool chamber is comstructed around the grips and functions as an insulator.

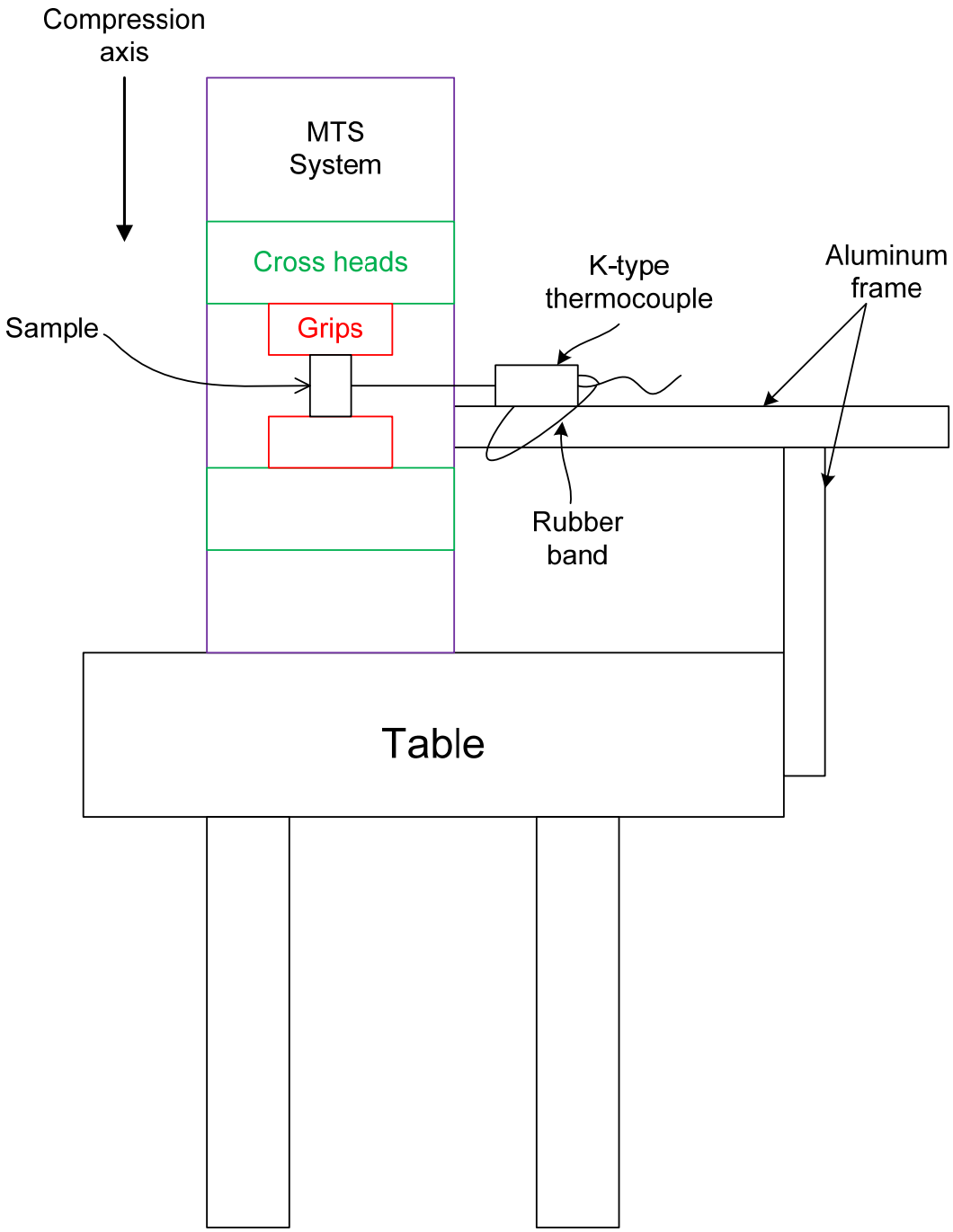

Figure 4-1 Schematic picture of the MTS compression system used for testing CoNiAl ferromagnetic SMAs

Thermo-Mechanical Response of $Co_{48}Ni_{33}Al_{29}$ Ferromagnetic SMA

Figure 4-2 demonstrates the strain-temperature response of $CoNi_{33}Al_{29}$ single crystal under various constant stresses levels from 25 MPa to 200 MPa. The stress was first applied at high temperature austenite phase. Then, the sample was thermally cycled between a temperature lower than M_f (around -30°C) and a temperature above A_f under constant stress. The first cycle was conducted under 25 MPa between -30°C and 80°C. When the first cycle was completed, stress was increased to a higher level and another cycle was repeated. Critical temperatures were determined using the same method as for NiMnCoIn alloy in the previous chapter (Figure 3-1). Transformation strain was taken as the strain value between M_f and M_s (Figure 3-1). Thermal hysteresis was defined as the temperature difference between the forward and reverse transformation at the middle of transformation strain level. All the critical temperatures and hysteresis were listed in Table 4-1.

Table 4-1 Isobaric thermal cycling results for $CoNi_{33}Al_{29}$ single crystals oriented along the [001] orientation

Stress (MPa)	Ms(°C)	Af(°C)	Transformation strain %	Thermal hysteresis (°C)
25	7.9	45.8	4.12	31.6
50	26.4	60.3	3.83	26.2
100	56.9	77.9	3.24	14.8
150	78.3	101.9	3.11	18.6
200	100.6	123.4	2.81	17.7

Three important observations are worth mentioning here. First, the Ms temperature and corresponding reverse transformation temperature increase with increasing applied stress. Such behavior is expected from Clauius-Clapeyron relation. Second, the transformation strain decreases with increasing stress. The reason for that will be discussed later. Third, the thermal hysteresis also decreases at high external stress, which will also be explained in the next section.

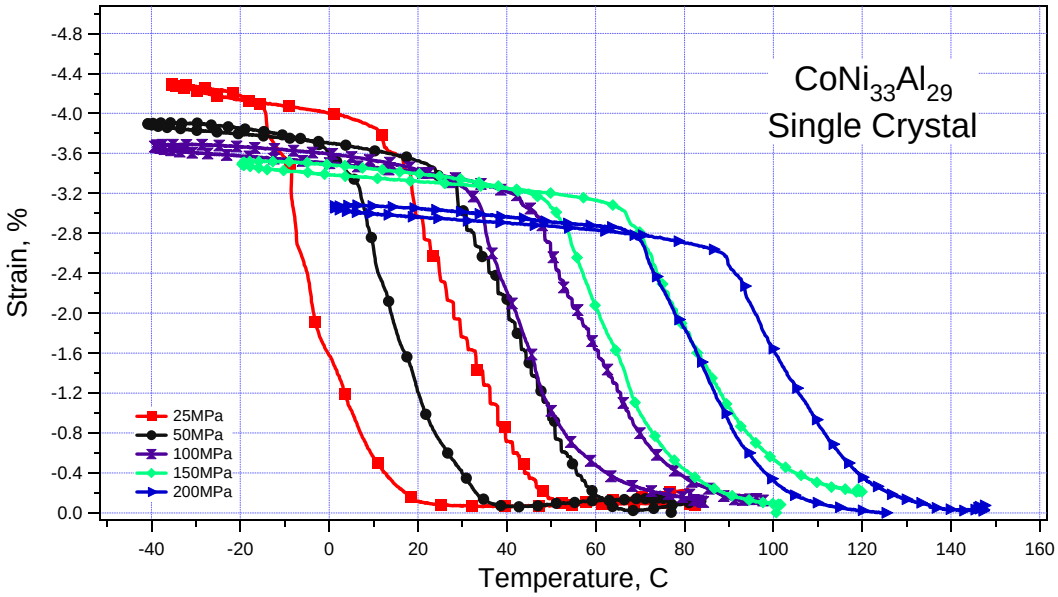

Figure 4-2 Isobaric thermal cycling experiments for $CoNi_{33}Al_{29}$ single crystal

Figure 4-3 shows the stress-strain response as a function of temperature. Displacement control is used during loading and the rate of loading is 0.004 mm/s, while force control was used for unloading at the rate of 20 N/s. The reason for using different control method in loading and unloading is mainly due to the experimental difficulties. For displacement control, an upper or lower limit of displacement must be specified. However, it is extremely difficult to determine the lower limit for unloading before the test due to uncertainty on pseudoelastic response. Although different methods were used for loading and unloading, it is consistent for all the tests so that the results are still

considered to be representative the nature of the material.

Pseudoelastic experiments were conducted from 35°C to 175°C and the results show perfect response behaviors in Figure 4-3 at these temperature. Critical stress for the onset of martensite phase transformation increases with temperature. For each test, sample was loaded further after martensitic transformation is corrected into the elastic region of martensite so that the elastic modulus of martensite could be determined at different temperatures. Although not clear enough from the figure, stress hysteresis and transformation strain both slightly decrease with temperature. All the critical parameters extracted from these experiments are shown in Table 4-2. The way of taking transformation strain is the same as mentioned in the last chapter (Figure 3-18). Stress hysteresis is taken from the stress difference between loading and unloading curve at the middle value of transformation strain.

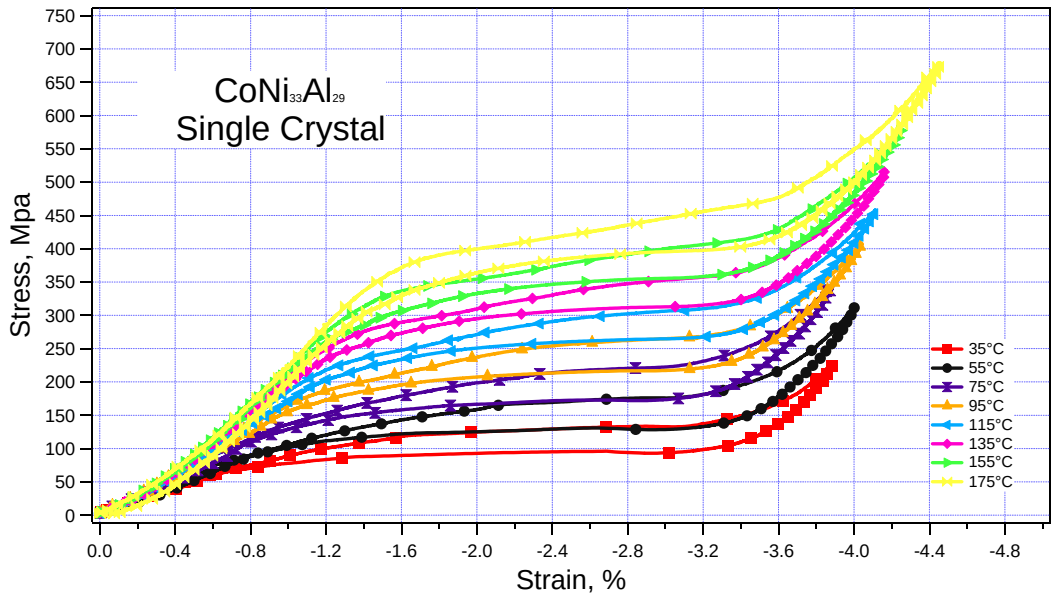

Figure 4-3 Pseudoelastic experiments on $CoNi_{33}Al_{29}$ single crystal from 35°C to 175°C show perfect pseudoelastic loops

Table 4-2 Transformation stress, strain, elastic modulus of austenite and martensite and stress hysteresis values recorded from pseudoelastic experiments of $CoNi_{33}Al_{29}$ single crystal

Temperature (°C)	Transformation stress(MPa)	Transformation strain%	Elastic Modulus of Austenite (GPa)	Elastic Modulus of Martensite (GPa)	Stress Hysteresis (MPa)
35	63.93	3.34	9.78	47.3	32.7
55	99.02	3.24	15.65	41.7	40.25
75	136.04	3	17.2	43.89	28.1
95	175.52	2.93	19.93	36.06	35.32
115	217.05	2.85	22.26	41.26	28
135	269.8	2.76	25.8	56.21	22.88
155	327.6	2.64	26.67	48.87	30.56
175	377.9	2.63	30.27	49.89	32.31

Effect of Loading Conditions on the Transformation Strain and Hysteresis of $Co_{48}Ni_{33}Al_{29}$ Shape Memory Alloys

Relation between transformation strain and compressive stress can be seen in Figure 4-4. Squares represent the transformation strain from the isobaric thermal cyclic tests (ε_{SME}) while circles show the transformation strain from the pseudoelastic tests (ε_{PE}). In order to compare ε_{SME} and ε_{PE}, critical stress for the martensitic transformation is employed for ε_{PE} instead of temperature and is added to the figure. It could be observed that ε_{SME} and ε_{PE} values fit well with each other. Both of them show that the transformation strain decreases with increasing compressive stress. ε_{SME}

decreases slightly faster than ε_{PE}, as indicated by the blue dash line in the figure. This is probably because of the error when taking critical stress at different temperature.

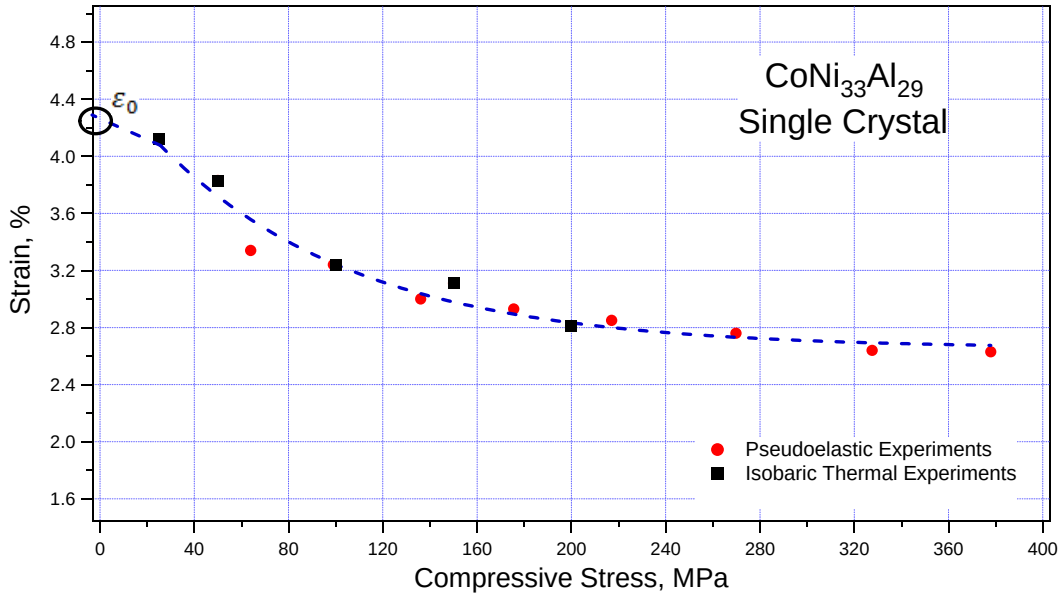

Figure 4-4 Experimental transformation strain versus compressive stress on $CoNi_{33}Al_{29}$ single crystal

Transformation strain decreases with compressive stress for this material. However, there is an "anomaly" in the relation between transformation strain and compressive stress for different materials. For example, transformation strain does not change notably with increasing stress for near equiatomic NiTi [57]. On the other hand, transformation strain decreases with increasing stress in NiFeGa [55]. Moreover, such "anomaly" is even single crystal orientation and crystallographic texture dependent. Here, to better understand the mechanism behind this, it is hypothesized that the decrease in transformation strain with increasing stress or temperature should be related to the uneven variation in lattice constants of austenite and martensite under stress or temperature. Neglecting the change in lattice parameters with temperature, a simple calculation can be conducted to take the effect of stress into account on the

transformation strain.

$$\varepsilon = \varepsilon_0 - \frac{\sigma_c}{E_A^T} + \frac{\sigma_c}{E_M^T} \quad 4\text{-}1$$

where ε is the transformation strain from experiments, either ε_{SME} or ε_{PE}. ε_0 is taken by extrapolating the dash line with ε_{SME} values to strain axis in Figure 4-4 and the correspondent value is 4.3%. It should be mentioned that ε_0 is not the real transformation strain under zero stress. Instead it is just an imagined mathematic value to show the transformation strain without taking stress into account. E_A^T is the Young's modulus of austenite and E_M^T is the Young's modulus of martensite at temperature T. σ_c is the critical stress for transformation. At 35°C, the equation can be written as follows:

$$\varepsilon = 4.3\% - \frac{63.93MPa}{9.78GPa} + \frac{63.93MPa}{47.3GPa} = 3.78\%$$

The experimental value at 35°C is 3.34%, which is close to the calculated results. The deviation is probably because of neglecting the change of lattice parameters from temperature change.

To better verify the assumption on the effect of variation in lattice constants on transformation strain, the reverse calculation is performed based on the experimental results, in which case ε_0 is calculated from the experimental transformation strain at various temperatures. The elastic modulus of austenite and martensite are taken from Table 4-1 and 4-2. The calculation results are shown in figure 4-5.

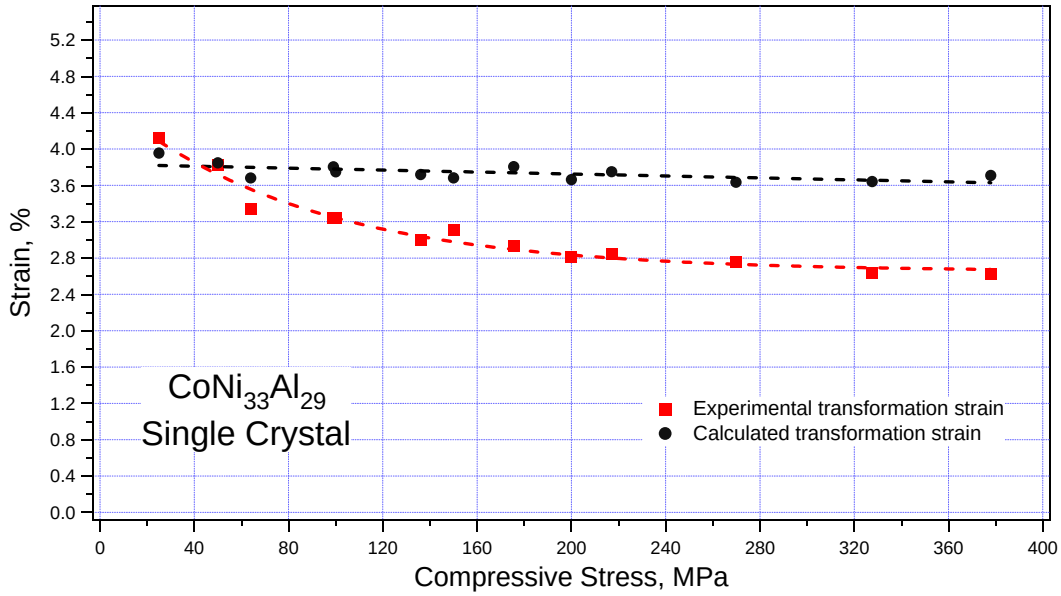

Figure 4-5 Experimental transformation strain and the calculated transformation strain on $CoNi_{33}Al_{29}$

As shown by the black curve (calculated transformation strain) in figure 4-5, without taking the variation of lattice constant change in austenite and martensite, it could be seen that the transformation strain is less influenced by compressive stress. The calculated transformation strain remains almost constant as a function of compressive stress. A more general expression could be raised if we rearrange equation 4-1:

$$\frac{\varepsilon_0-\varepsilon}{\sigma_c}=\frac{1}{E_A^T}-\frac{1}{E_M^T}=\frac{E_M^T-E_A^T}{E_A^T\cdot E_M^T} \quad 4\text{-}2$$

Mathematically, since σ_c, E_A^T and E_M^T are always positive, $\varepsilon_0-\varepsilon$ and $E_M^T-E_A^T$ should be positive or negative at the same time. In other words, transformation strain tends to drop with respect to ε_0 at a temperature when the elastic modulus of martensite is larger than that of austenite at that temperature. In the present study, the elastic modulus of martensite is always larger than that of austenite. As a result, $\varepsilon_0-\varepsilon$ is always larger than zero. In other words, the transformation strain without considering the variation of lattice constant change is always larger than the experimental transformation strain, as shown in Figure 4-5. Moreover, since the critical stress increases much faster than elastic modulus with increasing temperature, the value of $\varepsilon_0-\varepsilon$ is likely to

increase with compressive stress. This explains the trend of the experimental transformation strain shown in Figure 4-4. Similarly, the pronounced change in transformation strain in NiFeGa and other Cobalt based SMAs is also due to the lower Young's modulus of austenite compared to that of martensite [55]. For the case of NiTi, transformation strain does not change a lot due to the small difference of the elastic modulus of the two phases [57].

Using equation 4-2, it is also possible to predict the change in transformation strain as a function of temperature. When σ_c is moved to the right hand side of the equation, left hand side of the equation will simply mean the change in transformation strain with reference to ε_0. All the terms in right hand side are temperature dependent. However, critical stress increases much faster than elastic modulus of the phases with increasing temperature. From table 4-2, the critical stress at 175°C is 377.9 MPa, which is about six times as much as the value at 35°C (63.93MPa), while for the same temperature difference, the elastic modulus of martensite only increases about 5% and elastic modulus of austenite just three times higher than at 35°C. These numbers suggest that the critical stress plays a dominant role in determining the change in transformation strain as a function of temperature. It is reasonable to predict this change using the change of critical stress with increasing temperature. Since critical stress increases with increasing temperature, the difference between the transformation strains is getting larger with increasing temperature. In other words, transformation strain decreases with increasing temperature, which matches the experimental results as shown in Figure 4-6.

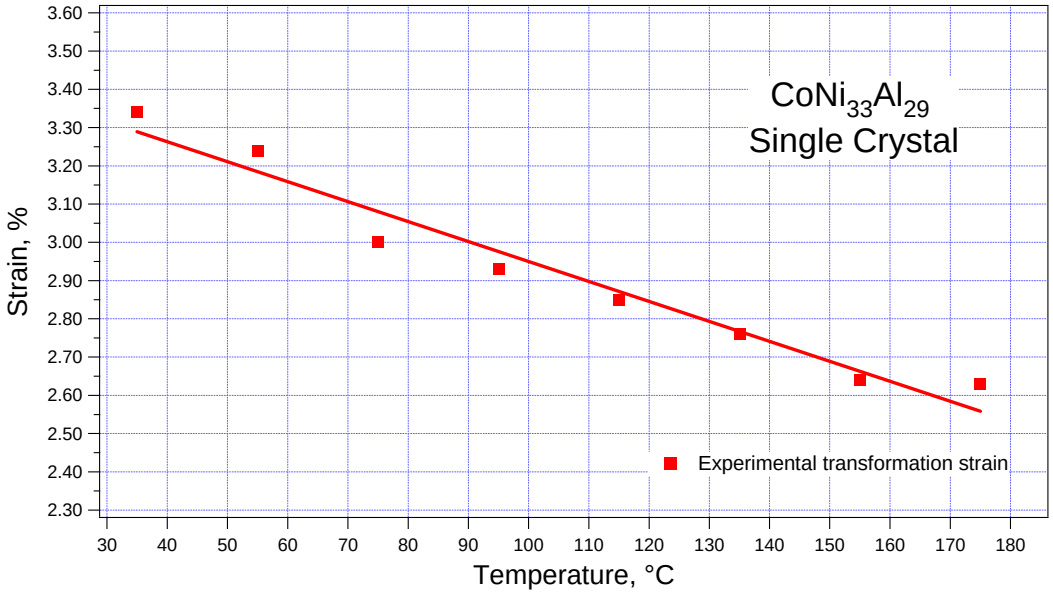

Figure 4-6 Experimental transformation strain versus temperature of $CoNi_{33}Al_{29}$

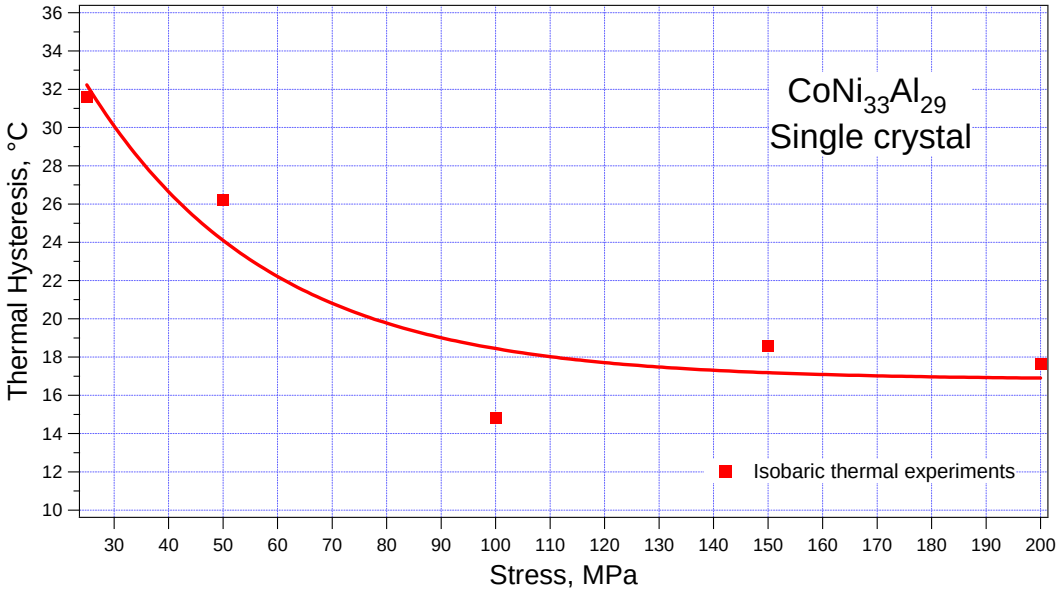

Figure 4-7 Thermal hysteresis versus applied stress of $CoNi_{33}Al_{29}$ single crystal

Transformation hysteresis is an important characteristics of SMAs because it is a measure of dissipated energy during temperature or stress cycling. As mentioned in the previous section, temperature hysteresis decreases with increasing applied stress in the [001] oriented $CoNi_{33}Al_{29}$ single crystals, as shown in Figure 4-7.

The results extracted from the isobaric thermal experiments are exponentially fit. Thermal hysteresis of the sample is about 32°C under 25 MPa and gradually decreases to around 18°C up to 200 MPa. Opposite trend was observed in CuZnAl and solutionized or overaged NiTi single crystals [63-65]. It was reported that the increasing thermal hysteresis with increasing applied stress originates from the partial accommodation during martensitic transformation by dislocations and other defects instead of elastic distortion of the matrix [66]. With increasing stress, the formation of dislocations becomes easier and thus leading to a larger hysteresis. On the other hand, the temperature hysteresis decreases with increasing applied stress in peak aged NiTi [67, 68]. The introduction of directional internal stress causes the decrease in thermal hysteresis [69]. In other words, the formation of dislocations in this case is more difficult than elastic distortion. This happens if the material is strong enough in parent phase so that more stress is required to form dislocations [25]. In the current study, the decreasing thermal hysteresis with increasing applied stress is also due to the dominating elastic distortion rather than dislocations for the accommodation. Moreover, two kinds of martensite are generated during martensitic transformation. They are stress-induced martensite and thermally-induced martensite, respectively. Variant-variant interaction between single variant stress-induced martensite and thermally-induced martensite happens and leads to energy dissipation during martensitic transformation, thus increasing the hysteresis. The volume fraction of stress-induced martensite increases at the expense of thermally-induced martensite at high stress level, which leads to lower level variant-variant interaction and decreases the energy dissipated. As a result, temperature hysteresis decreases at high applied stress level. It is also worth noting that the elastic modulus of austenite increases with increasing temperature. This means that the elastic stored energy in martensite plates and interfaces during martensite

transformation increases with increasing temperature. According to the Clausius-Clapyeron relation, critical stress for phase transformation increases with temperature, and vice versa, which indicates that more elastic stored energy should exist at high applied stress levels assuming the dissipation does not also increase with stress. Equation 1-1 shows that elastic energy stored during martensitic transformation thermodynamically favors the reverse transformation. This could be another reason for the decreasing temperature hysteresis with increasing applied stress.

Stress hysteresis also decreases with increasing temperature according to the results from the pseudoelastic experiments, as shown in Figure 4-8. The reason for such decrease is similar as discussed before for the thermal hysteresis. Moreover, Cui *et al* [70] related the transformation hysteresis in SMAs to crystalline symmetry and geometric compatibilities. The decreasing stress hysteresis in the current study for $Co_{48}Ni_{33}Al_{29}$ single crystal may also indicate a better compatibility at high temperatures than that at low temperature. According to Cui *et al.*, assuming no volume change during transformation, the hysteresis is dependent on how close the middle eigenvalue of the transformation matrix is to one. They also pointed out that in such an ideal case the whole martensite region will consist of only one variant. As discussed in the introduction section, martensite transformation could be decomposed of three parts in terms of phenomenological crystallographic theory. They are Bain distortion, rigid body rotation and a lattice invarient shear. The transformation matrix mentioned above is exactly the Bain distortion. In other word, the idea reported by Cui *et al* could be understood that the compatibility will reach the perfect condition when martensite transformation can be performed by Bain distortion alone, which is reasonable. According to the current results on $Co_{48}Ni_{33}Al_{29}$ single crystals, the lattice parameters of austenite and martensite changes unevenly due to different elastic modulus of austenite and martensite. Since the elastic modulus of austenite and martensite also changes unevenly, the compatibility of austenite and martensite phase gets much better at high temperatures, such that the stress hysteresis decreases with increasing temperature.

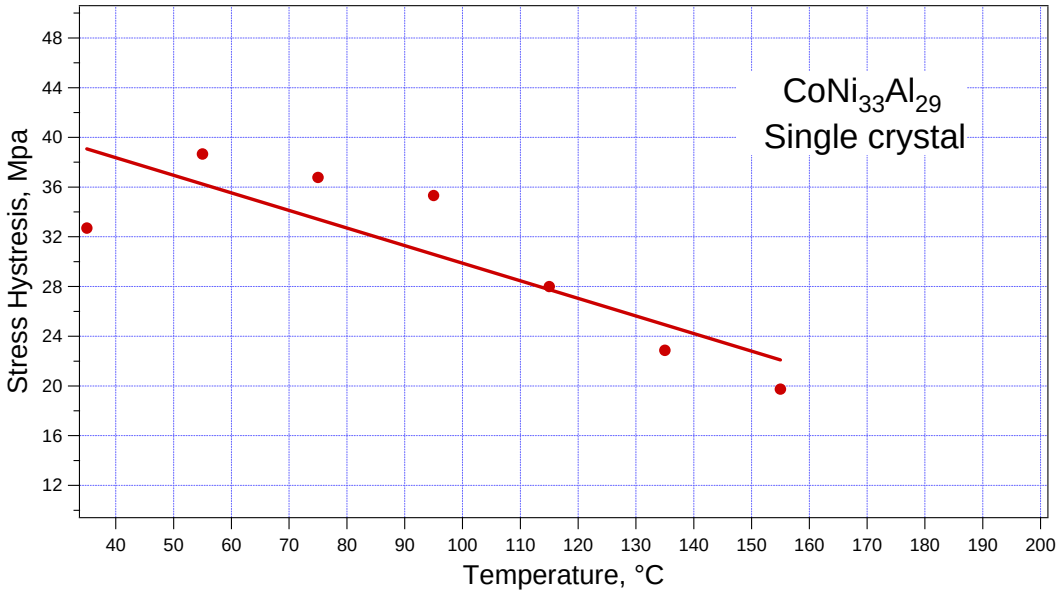

Figure 4-8 Stress hysteresis versus temperature of $CoNi_{33}Al_{29}$ single crystal, which shows a decreasing trend with increasing temperature

CHAPTER V
CONCLUSIONS

In the present work, $Ni_{45}Mn_{36.5}Co_5In_{13.5}$ single crystalline samples with the [001] and [111] orientation were homogenized at 900°C for 24 hours and cooled through water quenching, oil quenching and furnace cooling. The following conclusions can be reached after X-ray diffraction analysis, SQUID magnetometer and magnetic-thermo-mechanical experiments.

1. The slope of the curves in the stress versus temperature phase diagram is orientation dependent. The critical stress for the onset of martensitic transformation for the [111] oriented samples increase faster with temperature than those for the [001] oriented samples. The Claussius-Clapeyron relationship governs this trend and the smaller achievable strain of the [111] oriented samples accounts for the larger slope.
2. The furnace cooled samples have the lowest Ms temperatures and water quenched samples have the highest Ms temperatures. Crystallographic orientation does not seem to affect Ms temperature.
3. Heat treatment influences the atomic ordering of sample. The water quenched sample has a $L2_1$ austenite structure and 12M modulated martensite phase. The oil quenched sample has a mixture structure in both austenite and martensite phases. The furnace cooled sample does not show any martensitic transformation in X-ray diffraction and SQUID upon cooling under zero stress and field. The reason for these observation is not clear.
4. Magnetostress is dependent on the orientation, temperature and heat treatment of the samples. The [111] oriented samples have a higher magnetostress than the [001] oriented samples. The low achievable strain of the [111] oriented samples is thought to be the reason for such observation. For samples with same orientation, temperature affects the magnetostress due to the change in magnetization difference between austenite and martenstie phases at different temperatures. Moreover,

magnetostress is heat treatment dependent, which is due to the change in magnetic properties as a results of different atomic ordering.

5. Temperature affects the magnetostress of $Ni_{45}Mn_{36.5}Co_5In_{13.5}$ single crystals. Magnetostress tends to decrease when the operating temperature of the superelastic experiments is approaching the Curie temperature.
6. Stress-assisted reversible magnetic field induced martensitic transformation could not be achieved in the [001] furnace cooled $Ni_{45}Mn_{36.5}Co_5In_{13.5}$ single crystals. This is because the magnetostress under 1.6T available field is not strong enough to compensate for the energy dissipated during transformation.

In addition, the [001] oriented $CoNi_{33}Al_{29}$ single crystals were also investigated to examine the effect of thermo-mechanical loading condition on the transformation strain and hysteresis. The following conclusions come from the thermo-mechanical experiments.

1. Perfect shape memory effect was observed in isobaric thermal cycling experiments under the applied stress levels up to 200 MPa. Complete pseudoelasticity was achieved up to 175°C with a 4.5% maximum strain.
2. Transformation strain decreases with increasing applied stress or temperature. The unevenly changed elastic modulus of austenite and martensite with increasing temperature attributes to such decrease in transformation strain.
3. Thermal hysteresis decreases with increasing constant applied stress.
4. Stress hysteresis also decreases with increasing temperature. The lattice parameters of austenite and martensite changes unevenly due to different elastic modulus of austenite and martensite, which probably improves the structure compatibility between martensite and austenite.

REFERENCES

[1] Park SE, Shrout TR. Journal of Applied Physics 1997;82:1804.

[2] Clark AE, Wun-Fogle M. Modern magnetostrictive materials - Classical and non-classical alloys. In: Proceedings of SPIE - The International Society for Optical Engineering 2002, 4699, p.421-436.

[3] Clark AE, Restorff JB, Wun-Fogle M, Lograsso TA, Schlagel DL. IEEE-Inst Electrical Electronics Engineers Inc 2000, 36, p.3238-3240.

[4] Funakubo H. Shape memory alloys. Amsterdam: Gordon & Breach Publishing Group;1987.

[5] Lazarus D. Physical Review 1949;76:545.

[6] Klier EP, Grymko SM. Transactions of the American Institute of Mining and Metallurgical Engineers 1949;185:611.

[7] Lieberman DS, Wechsler MS, Read TA. Journal of Applied Physics 1955;26:473.

[8] Otsuka K, Ren X. Progress in Materials Science 2005;50:511.

[9] Sehitoglu H, Karaman I, Anderson R, Zhang X, Gall K, Maier HJ, Chumlyakov Y. Acta Mater. 2000;48:3311.

[10] CM. Wayman and HKDH. Bhadeshia. Physical Metallurgy, edited by RW. Cahn and P. Haasen. Amsterdam: North Holland; 1996.

[11] Bain EC. Transactions of the American Institute of Mining and Metallurgical Engineers 1924;70:25.

[12] Christian JW. Metallurgical Transactions a-Physical Metallurgy and Materials Science 1982;13:509.

[13] Karaca HE, Karaman I, Basaran B, Chumlyakov YI, Maier HJ. Acta Mater. 2006;54:233.

[14] Karaca HE, Karaman I, Basaran B, Lagoudas DC, Chumlyakov YI, Maier HJ. Scripta Materialia 2006;55:803.

[15] Ullakko K, Huang JK, Kantner C, O'Handley RC, Kokorin VV. Appl. Phys. Lett. 1996;69:1966.

[16] Otsuka KW, CM. Wayman. Shape memory materials. New York; Cambridge University Press; 1998.

[17] Heczko O, Straka L. Materials Science and Engineering A 2004;378:394.

[18] Karaman I, Karaca HE, Basaran B, Lagoudas DC, Chumlyakov YI, Maier HJ. Scripta Materialia 2006;55:403.

[19] O'handley RC. Modern magnetic materials: principles and applications. New York: John Wiley & Sons;2000.

[20] Henry CP, Bono D, Feuchtwanger J, Allen SM, Handley RC. J. Appl. Phys. 2002, 91:10.

[21] Sozinov A, Likhachev AA, Ullakko K. IEEE Transactions on Magnetics 2002;38:2814.

[22] Kainuma R, Nakano H, Ishida K. Metallurgical and Materials Transactions A: Physical Metallurgy and Materials Science 1996;27:4153.

[23] Kainuma R, Ito W, Umetsu RY, Oikawa K, Ishida K. Appl. Phys. Lett. 2008;93.

[24] Karaca HE, Karaman I, Lagoudas DC, Maier HJ, Chumlyakov YI. Scripta Materialia 2003;49:831.

[25] Karaca HE, Karaman I, Chumlyakov YI, Lagoudas DC, Zhang X. Scripta Materialia 2004;51:261.

[26] Sato M, Okazaki T, Furuya Y, Kubota T, Saito C, Wuttig M. Nippon Kinzoku Gakkaishi/Journal of the Japan Institute of Metals 2002;66:147.

[27] Kishi Y, De Graef M, Craciunescu C, Lograsso TA, Neumann DA, Wuttig M. Journal De Physique. IV. 2003;112:1021.

[28] Hamilton RF, Efstathiou C, Sehitoglu H, Chumlyakov Y. Scripta Materialia 2006;54:465.

[29] Dadda J, Maier HJ, Karaman I, Karaca HE, Chumlyakov YI. Scripta Materialia 2006;55:663.

[30] Dadda J, Maier HJ, Niklasch D, Karaman I, Karaca HE, Chumlyakov YI. Metallurgical and Materials Transactions a-Physical Metallurgy and Materials Science 2008;39A:2026.

[31] Kainuma R, Imano Y, Ito W, Sutou Y, Morito H, Okamoto S, Kitakami O, Oikawa K, Fujita A, Kanomata T, Ishida K. Nature 2006;439:957.

[32] Karaca HE, Karaman I, Basaran B, Lagoudas DC, Chumlyakov YI, Maier HJ. Acta Materialia 2007;55:4253.

[33] O'Handley RC, Murray SJ, Marioni M, Nembach H, Allen SM. J. Appl. Phys. 2000;87:4712.

[34] Krenke T, Acet M, Wassermann EF, Moya X, Manosa L, Planes A. Physical Review B - Condensed Matter and Materials Physics 2006;73.

[35] Chatterjee S, Giri S, Majumdar S, De SK. Physica B-Condensed Matter 2008;403:2572.

[36] Pathak AK, Gautam BR, Dubenko I, Khan M, Stadler S, Ali N. J. Appl. Phys. 2008; 103(7): 07F315.

[37] Pathak AK, Khan M, Dubenko I, Stadler S, Ali N. Applied Physics Letters 2007;90:3.

[38] Kainuma R, Oikawa K, Ito W, Sutou Y, Kanomata T, Ishida K. Journal of Materials Chemistry 2008;18:1837.

[39] Umetsu RY, Kainuma R, Amako Y, Taniguchi Y, Kanomata T, Fukushima K, Fujita A, Oikawa K, Ishida K. Appl. Phys. Lett. 2008;93.

[40] Sutou Y, Imano Y, Koeda N, Omori T, Kainuma R, Ishida K, Oikawa K. Appl. Phys. Lett. 2004;85:4358.

[41] Pecharsky VK, Gschneidner KA. Physical Review Letters 1997;78:4494.

[42] Tegus O, Bruck E, Zhang L, Dagula, Buschow KHJ, De Boer FR. Physica B: Condensed Matter 2002;319:174.

[43] Liu ZH, Aksoy S, Acet M. J. Appl. Phys. 2009;105:5.

[44] Aksoy S, Yucel A, Elerman Y, Krenke T, Acet M, Moya X, Manosa L. Journal of Alloys and Compounds 2008;460:94.

[45] Jing C, Li Z, Zhang HL, Chen JP, Qiao YF, Cao SX, Zhang JC. Eur. Phys. J. B 2009;67:193.

[46] Krenke T, Duman E, Acet M, Wassermann EF, Moya X, Manosa L, Planes A. Nat. Mater. 2005;4:450.

[47] Pathak AK, Dubenko I, Mabon JC, Stadler S, Ali N. J. Phys. D-Appl. Phys. 2009;42:8.

[48] Kainuma R, Imano Y, Ito W, Morito H, Sutou Y, Oikawa K, Fujita A, Ishida K, Okamoto S, Kitakami O, Kanomata T. Appl. Phys. Lett. 2006;88.

[49] G.Bertotti. Hysteresis in Magnetism. San Diego: Academic Press;1998.

[50] Fischer FD, Berveiller M, Tanaka K, Oberaigner ER. Archive of Applied Mechanics 1994;64:54.

[51] Bhattacharya. Microstructure of martensite. New York:Oxford University Press;2003.

[52] Lovey FC, Torra V. Progress in Materials Science 1999;44:189.

[53] Oikawa K, Wulff L, Iijima T, Gejima F, Ohmori T, Fujita A, Fukamichi K, Kainuma R, Ishida K. Appl. Phys. Lett. 2001;79:3290.

[54] Omori T, Kamiya N, Sutou Y, Oikawa K, Kainuma R, Ishida K. Materials Science and Engineering A 2004;378:403.

[55] Sutou Y, Kamiya N, Omori T, Kainuma R, Ishida K, Oikawa K. Appl. Phys. Lett. 2004;84:1275.

[56] Hamilton RF, Sehitoglu H, Efstathiou C, Maier HJ, Chumlyakov Y. Acta Mater. 2006;54:587.

[57] Shaw JA, Kyriakides S. Journal of the Mechanics and Physics of Solids 1995;43:1243.

[58] Ito W, Imano Y, Kainuma R, Sutou Y, Oikawa K, Ishida K. Metallurgical and Materials Transactions A-Physical Metallurgy and Materials Science 2007;38A:759.

[59] Ito W, Nagasako M, Umetsu RY, Kainuma R, Kanomata T, Ishida K. Appl. Phys. Lett. 2008;93.

[60] Haluk E. Karaca, Advanced Functional Materials 2009;19:983.

[61] Wang YD, Huang EW, Ren Y, Nie ZH, Wang G, Liu YD, Deng JN, Choo H, Liaw PK, Brown DE, Zuo L. Acta Mater. 2008;56:913.

[62] Ito W, Ito K, Umetsu RY, Kainuma R, Koyama K, Watanabe K, Fujita A, Oikawa K, Ishida K, Kanomata T. Appl. Phys. Lett. 2008;92.

[63] Liu Y, Tan G, Miyazaki S. Materials Science and Engineering A 2006;438-440:612.

[64] Kayali N, Zengin R, Adiguzel O. Metallurgical and Materials Transactions A: Physical Metallurgy and Materials Science 2000;31:349.

[65] Chernenko VA, L'Vov V, Pons J, Cesari E. J. Appl. Phys. 2003;93:2394.

[66] Chernenko VA, Pons J, Cesari E, Ishikawa K. Acta Mater. 2005;53:5071.

[67] Kajiwara S, Kikuchi T, Ogawa K, Matsunaga T, Miyazaki S. Philos. Mag. Lett. 1996;74:137.

[68] Fukuda T, Deguchi A, Kakeshita T, Saburi T. 1997: Japan Inst Metals. p.514.

[69] Hornbogen E. Acta Metallurgica 1985;33:595.

[70] Cui J, Chu YS, Famodu OO, Furuya Y, Hattrick-Simpers J, James RD, Ludwig A, Thienhaus S, Wuttig M, Zhang ZY, Takeuchi I. Nat. Mater. 2006;5:286.

VITA

Name: Ruixian Zhu

Address: Texas A&M University
Department of Mechanical Engineering
3123 TAMU
College Station TX 77843-3123

Email Address: zhuruixian@neo.tamu.edu

Education: B.S., Mechanical Engineering, Shanghai Jiao Tong University, 2007
M.S., Mechanical Engineering, Texas A&M University, 2009